Synthesis and Immobilization of an Iridium Complex for use in Enzymatic Biocatalysis

Master's Thesis

Submitted by:

Robin Frédéric Keller [21-103-726], January 30, 2026

In fulfillment of the degree "Master of Science in Molecular Life Sciences with special qualification in Biochemistry/Chemical Biology"

Supervisor:

Prof. Dr. Martin Albrecht

Department of Chemistry, Biochemistry and Pharmaceutical Sciences University of Bern, Freiestrasse 3, CH-3012 Bern (Switzerland).

Acknowledgements

First of all, I would like to thank my supervisor, Prof. Dr. Martin Albrecht, for giving me the opportunity to continue with my MSc thesis, after I had already conducted my BSc thesis in his group. Your insight, expertise, and continued support have been invaluable for this work and my career as a critically thinking scientist.

I'd like to give special thanks to Laura C.G. Monte. Thank you for your continued support over these two years, both during my BSc thesis and now MSc thesis. Your help has been invaluable to me, both inside and outside the laboratory. I consider myself incredibly lucky to have found a capable mentor in you, and now also a very good friend.

I also want to thank all other members of the Albrecht group. Thank you for all your help, be it directly in the laboratory, or through insightful discussions. I am also very grateful for the fun evenings filled with joy and laughter I could experience with each and every one of you.

Last but not least, I want to thank my family and friends who have supported me through these formative years in which I have pursued this degree. Thank you for your support and help during all these times.

Abstract

The combination of transition metal (TM) and enzymatic catalysis is advantageous due to the complementary nature of the two methods. However, systems combining TM catalysts and enzymes are rare and often suffer from mutual inhibition. If this mutual inhibition could be circumvented, many new synthetic procedures could be established. In this work, we present the synthesis and immobilization of an iridium catalyst to minimize said mutual inhibition. The synthesis of the iridium complex proved to be reliable and cheap, and we showed that we can reliably quantify the amount of immobilized catalyst. We employed the immobilized TM catalyst in the regeneration of NAD(P)H, and combined it with three NAD(P)H dependent enzymes. Immobilization leads to the reduction of mutual inhibition, as well as to the reuse of the TM catalyst. We also successfully employed the immobilized TM catalyst in flow, where it can be modularly combined with different immobilized NAD(P)H dependent enzymes. Our results provide a starting point for the industry to implement a simple and reliable immobilized TM system in combination with enzymatic procedures.

Content

1 Introduction

The combination of transition metal (TM) catalysis and enzymatic catalysis has raised interest in recent years.[1–4] The main goal of this field is to exploit the complementary advantages of both methods. TM catalysts often tolerate elevated temperatures and pressures, organic solvents, and a wide range of substrates.[5] On the other hand, enzymes are often stereo-, regio-, and enantioselective, and capable of catalysing reactions under relatively mild conditions.[6,7] This can render the catalysis more sustainable and cheaper, making it easier for the process to meet the "green chemistry" requirements.[8]

However, the combination of TM catalysts and enzymes has proven challenging, as there is often a mutually inhibitory effect.[9–13]Previous work suggests, that this inhibitory effect may arise from nucleophilic amino acid residues. Cysteine, histidine, and tryptophane are shown to be the most strongly inhibiting residues, possibly due to coordination to the metal centre. This coordination could in turn prevent the TM from undergoing a catalytic cycle, and also possibly affect the tertiary structure of the enzyme, reducing the activities of both catalysts.[10,11,14]

To mitigate mutual inhibition, compartmentalization of the two catalysts is commonly employed to reduce their direct interaction. Several approaches have been developed, such as a biphasic system, where the TM catalyst is confined in an organic phase, while the enzyme remains in an aqueous phase. This has been successfully employed in our previous work.[15] Another strategy involves the use of surfactants.[16] This technique is employed in ongoing research by Laura Monte. Another strategy to minimize catalyst interactions involves the use of deep eutectic solvents (DES). Pioneering work by the García-Álvarez group has shown a significant reduction in the mutual inhibition between the two catalysts.[17–19]

Recently, the Hollman group explored the covalent immobilization of both catalysts on a solid phase.[4] Immobilization of the enzyme has already been shown to be promising in reducing the mutual inhibition, due to the decreased possibilities for interactions between the catalysts by engaging nucleophilic amino acid residues in interactions with the resin.[4,11,14]

Immobilization of TM catalyst is a well-established strategy and several approaches have been developed to anchor catalysts onto solid supports. One of the first publications of immobilized TM catalysts on a resin came from Whitehurst and colleagues, who employed an ion-exchange resin to immobilize the catalyst.[20] In the following years, extensive research has been conducted on the immobilization of TM catalysts *via* different methods. A non-exhaustive list of methods includes: Immobilization of the complex *via* coordination to the solid support; Immobilization of the complex *via* ionic interactions with the solid support; Immobilization of the complex *via* covalent binding of the ligand to the solid support; Non-permanent immobilization of the complex to the solid support *via* a proposed boomerang-mechanism.[21–30]

Immobilization of the TM catalysts offers several advantages, notably enabling catalyst reuse. Upon the catalysis of a reaction by an immobilized TM catalyst, the medium can be readily separated from the catalyst by filtration, allowing catalyst recovery and reuse.

Despite the well-established nature of TM catalyst immobilization, their use in industrial application is rare.[31] A major disadvantage includes the unpredictability in the catalytic activity after immobilization.[24,26] Another major drawback is catalyst leaching, which results in two significant limitations. Leaching of the metal will require additional purification steps to remove the heavy metal contaminants from the final product.[22,24,25] Additionally, loss of the immobilized metal catalyst leads to a degradation of the catalytic activity over time.

Besides TM catalysts being immobilized, enzymes can also be immobilized, to further prevent interactions between the two catalysts. Four techniques (Figure 1) can be employed for the immobilization of enzymes: **I** Adsorption; **II** Covalent bonding; **III** Entrapment; **IV** Cross-linking.[32,33]

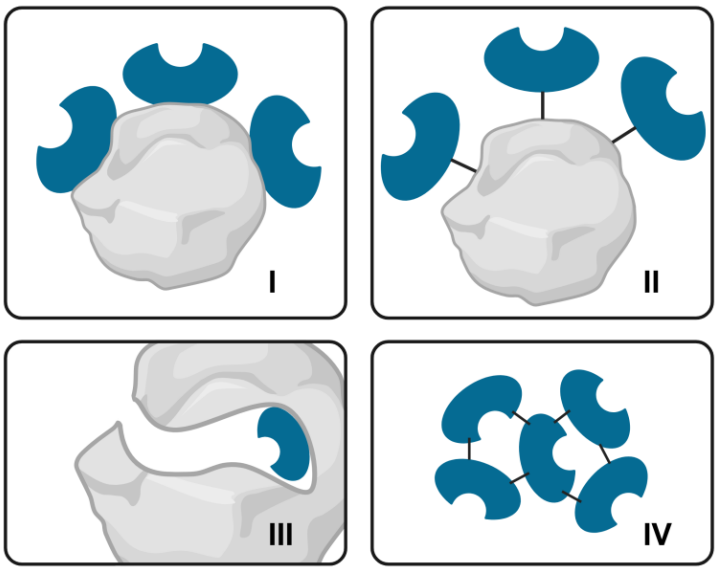

Figure 1: The schematic immobilization of an enzyme (blue) *via*: **I** Adsorption; **II** Covalent bonding; **III** Entrapment; **IV** Cross-linking. Created in https://BioRender.com

This immobilization brings several advantages, some similar to the immobilization of transition metal catalysts:

First, the immobilization allows for the reuse of the immobilized enzyme over several reactions. This is advantageous for the biocatalytic synthetic industry, as it can lower cost and improve process sustainability.

Second, immobilization of the enzyme can increase its stability.[34] The higher rigidity of the immobilized enzyme after the binding of the enzyme to the support can stabilize the enzymatic structure, potentially making it less prone to denaturation.[35,36] This enhanced stability can even allow the enzyme to function in organic solvents and elevated temperatures.[37]

Third, immobilization offers the options of tuning catalytic performance by employing different solid supports. For this, the choice of material of the solid support is a critical factor. An accurate choice can not only result in a good performance but also in a sustainable process.[38] Gelati et al. recently showed promising results by immobilizing three model enzymes on calcium hydroxyapatite, a cheap, sustainable, and biocompatible solid support.[39]

Due to these above-mentioned properties, industrial applications of immobilized enzymes have become more and more common.[40–43]

However, some drawbacks need to be pointed out. Immobilized enzymes often suffer from a reduced TOF which can be explained by the restricted movement of the immobilized enzyme. As enzymes need to be flexible during their reaction, to accommodate both the substrate and subsequently the product, the added rigidity can hinder the enzyme from properly catalysing the reaction. Additionally, similar to immobilized TM complexes, enzymes can also be prone to leaching, especially when immobilized *via* adsorption.[44,45]

In this work, we aim to immobilize the TM catalyst using chemistry and resins, commonly used for enzymes. This will lead to better compatibility between the two systems by reducing mutual inhibition. The employment of bioorthogonal resins could enable co-immobilization of both catalysts in future work.

As a case study, we worked on "nicotinamide adenine dinucleotide (phosphate)" (NAD(P)H) dependent enzymes. These enzymes often catalyse a reduction of a substrate, where NAD(P)H acts as a reductant donating a hydride to the substrate.

NAD(P)H is an enzymatic cofactor, which exists in all cells and functions as an electron carrier.

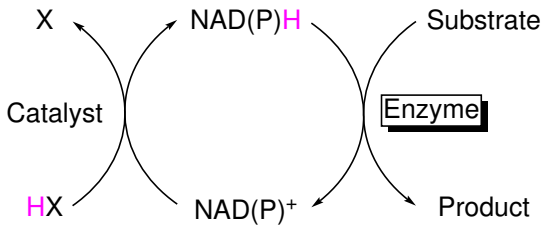

Scheme 1: A schematic representation of an enzymatic reaction relying on the cofactor NAD(P)H. The cofactor is present in a catalytic manner and is regenerated *via* a catalyst using a sacrificial hydride source.

The high cost of NAD(P)H, as well as its low stability at acidic pH and elevated temperatures, represents a major limitation for large-scale applications.[46] As a result, it is desirable to employ sub-stoichiometric amounts of NAD(P)H and to regenerate it *in-situ* during the catalytic process. A common strategy involves enzymatic regeneration of NAD(P)H using auxiliary dehydrogenases, such as glucose dehydrogenases from *Bacillus megaterium* or *Bacillus subtilis*.[47] In these systems, glucose is used as a sacrificial hydride donor, a cheap, renewable, and abundant resource. However, the introduction of an additional biocatalyst increases the complexity of the system, as both enzymes must operate under the same reaction conditions.

NAD(P)H can also be regenerated electrochemically. Recent research highlights the improvements of electrodes and the use of renewable energy in the process, making the approach desirable for industrial applications.[48–50]

The most relevant approach for this work is the regeneration of NAD(P)H *via* TM catalysis. An early example by Ruppert et al. employed a bypridine rhodium redox-catalyst for the regeneration of NAD(P)H (Scheme 2**I**).[51] They were able to supply the coupled lactate dehydrogenase

with NAD(P)H, allowing it to reduce its substrate pyruvate into D-lactate. This catalyst has become the standard catalyst for NAD(P)H regeneration.

The state-of-the-art TM catalysts for NAD(P)H regeneration have been developed by the Macchioni group.[52–55] In their most recent work they claim to have developed a catalyst (Scheme 2**II**) that reaches similar TOF as NADH regenerating enzymes, with 13090 h^{-1}.[54]

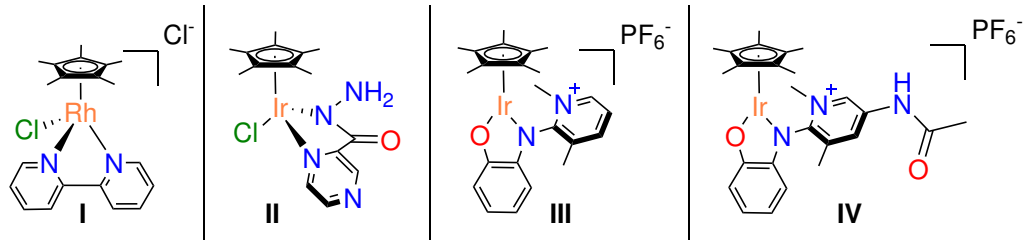

Scheme 2: The structures of: **I** [Cp*(Me)$_5$Rh(bipy)Cl]Cl[51]; **II** [Cp*Ir(κ^2-pyrazinecarbohydrazide)Cl][54]; **III** IrPYE[56]; **IV** IrPYE-Acetamide (by Laura Monte).

In this work, an iridium catalyst is employed to regenerate NAD(P)H. The catalyst is a variant of a previously published iridium complex containing a PYE-type ligand (Scheme 2**III**).[56] This catalyst, containing two methyl groups, stored the hydride on the N-heterocycle, bearing resemblance to NAD(P)H. Yet unpublished work by Sabela Reuge suggests, that first the metal-hydride complex is formed, then the hydride is transferred onto the ligand through a rapid intramolecular rearrangement. This complex has been shown to regenerate NADH, albeit only in DMSO.[57] Hydride storage on the ligand is not typical for TM catalysts, as most tend to form stable metal-hydride complexes instead.[58] In unpublished work by Laura Monte, the complex was further modified to contain an acetamide group (Scheme 2**IV**), increasing its solubility in aqueous solutions, as well as its activity towards NAD(P)$^+$. It was then employed for the catalytic regeneration of NAD(P)H from NAD(P)$^+$, *via* transfer hydrogenation.

In this work, we employ a variant of these in-house IrPYE complexes. We hypothesize that the robust metal centre, which limits undesired coordination, would reduce the mutual inhibition between the enzyme and TM catalyst. Additionally, it was chosen due to its stability and activity in aqueous solutions.

Another advantage of the chosen catalyst is the modularity of the ligand. Many starting materials are readily available, enabling the synthesis of many ligand variants. The idea in this work is to synthesize a ligand with an electrophilic functional group, working as a leaving group. This would allow the covalent immobilization of the iridium complex *via* the ligand on a resin bearing a nucleophile.

Aim of this thesis

This work aims to combine a covalently immobilized iridium catalyst and enzymes. For this purpose, a first step is the synthesis of an IrPYE-variant, which can be covalently immobilized on a variety of different resins, yielding ^{Ir}Resins (Scheme 3). The ^{Ir}Resins must be capable of NAD(P)H regeneration in aqueous solutions. They must additionally be reusable over multiple cycles, enhancing the sustainability of the process.

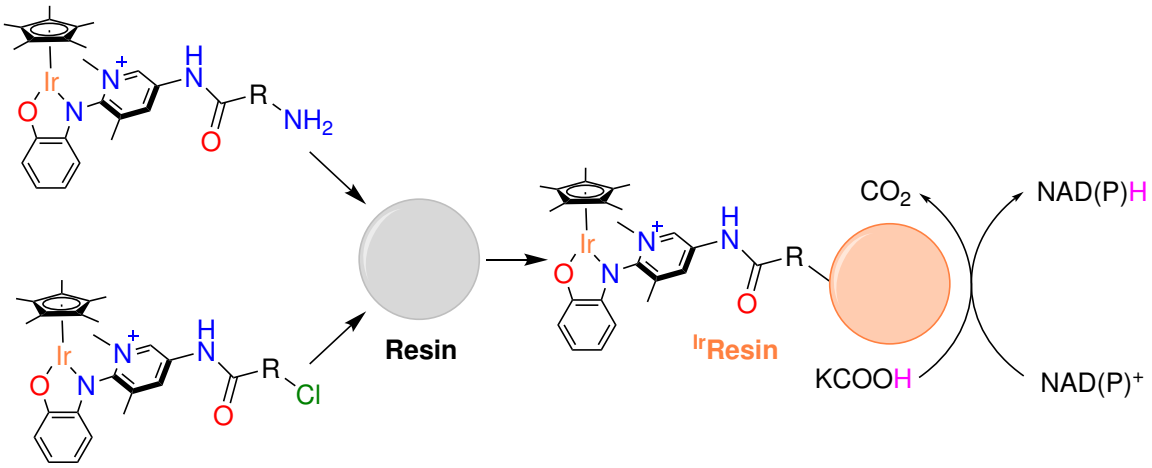

Scheme 3: The schematic immobilization of a nucleophilic IrPYE-variant bearing an α−NH_2 group, or an electrophilic IrPYE-variant bearing an α−Cl, on a resin. The ^{Ir}Resin is subsequently employed for the regeneration of NAD(P)H over multiple cycles.

Once an optimized system for the regeneration of NAD(P)H has been established, the ^{Ir}Resins will be coupled with enzymes in batch reactions (Scheme 4) and in flow. Combining both catalysts should result in the enantiopure product. Additionally, due to this immobilization of the TM complex, we hypothesize a decrease in the mutual inhibition seen both in literature, and our previous work.

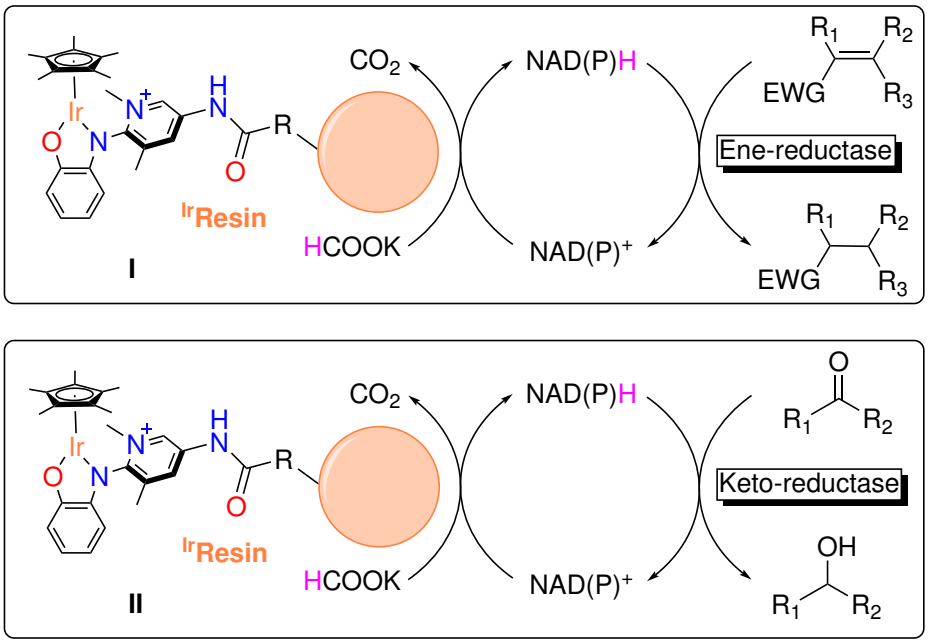

Scheme 4: The schematic combination of an ^{Ir}Resin for the purpose of NAD(P)H regeneration, allowing for: **I** enzymatic alkene reduction *via* an ene-reductase; **II** enzymatic ketone reduction *via* a keto-reductase.

2 Results and Discussion

2.1 Synthesis overview

We attempted to synthesize two different IrPYE variants (Scheme 5). One variant bearing an electrophilic moiety, which could function as a leaving group, and one bearing a nucleophilic moiety. This would allow for different types of immobilization chemistries, as well as different types of solid supports. In this chapter we show the synthesis of complexes bearing ligands with an electrophilic moiety, and discuss the limitations and difficulties of the synthesis of complexes bearing nucleophilic moieties.

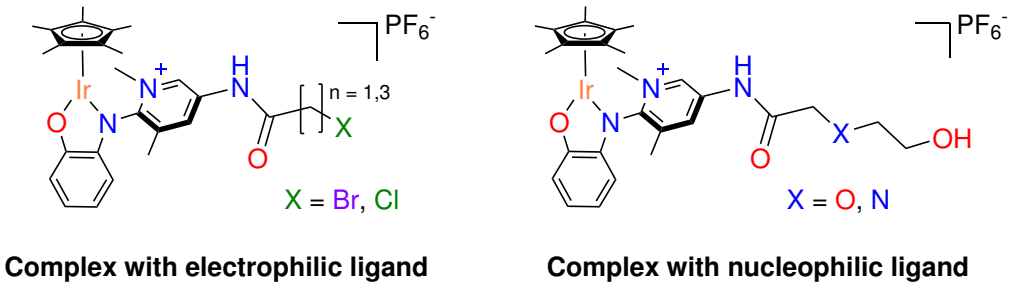

Complex with electrophilic ligand **Complex with nucleophilic ligand**

Scheme 5: The schematic representations of the two desired types of complexes, the electrophilic (left) and nucleophilic (right) complexes.

2.2 Synthesis of electrophilic complexes

2.2.1 Synthesis of the ligand precursor compound 1

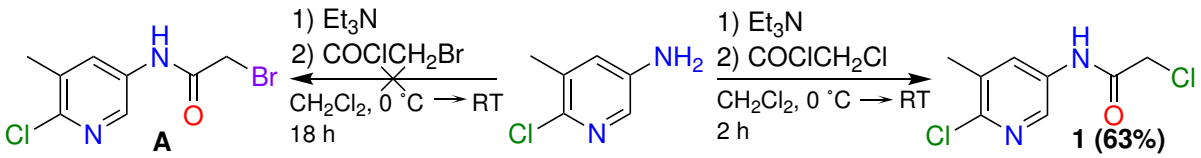

Scheme 6: Synthesis of compound **1** and related synthetic pathways.

The approach for the synthesis of the ligand was to mimic synthetic procedures that were already proven successful for other IrPYE variants. In previous work, Laura Monte used acetyl chloride in the first step of the PYE-Acetamide ligand. In an attempt to access a bromide as a leaving group, bromoacetyl chloride was employed as a substitute for acetyl chloride, attempting to synthesize compound **A**. ^{1}H NMR spectroscopy suggested several side reactions, therefore necessitating a different approach.

Hence, chloroacetyl chloride was instead used as a substitute for acetyl chloride. We could synthesize compound **1** (63%) *via* an S_N2 reaction with 6-chloro-5-methylpridin-3-amine. Compound **1** was fully characterized.

2.2.2 Synthesis of compound 4 (IrPYE-Cl)

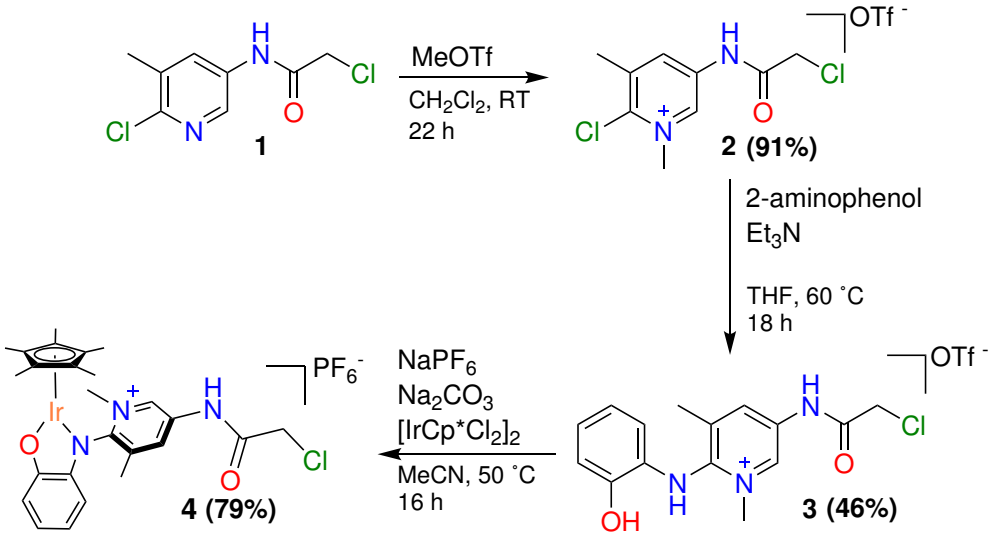

Scheme 7: Synthesis of compound **4** (IrPYE-Cl).

We again aimed to mimic established procedures. Therefore, we methylated compound **1** with MeOTf. This afforded compound **2** (91%) in high yield and purity. Compound **2** was fully characterized.

We next aimed for an S_NAr reaction on compound **2**, attempting to synthesize the electrophilic ligand, compound **3**. The 2-aminophenol was attached, resulting in compound **3** (46%), which was fully characterized.

In a last step, compound **4** was synthesized *via* complexation of compound **3** to $[IrCp^*Cl_2]_2$. This reaction afforded compound **4** (IrPYE-Cl) (79%) in high purity and yield. IrPYE-Cl was fully characterized. The typical Cp* signal at 1.69 ppm, the two methyl signals at 2.11 and 3.98 ppm, the methylene signal at 4.42 ppm, as well as the characteristic aromatic heterocycle signals at 8.66 and 9.40 ppm were all observed in the ^{1}H NMR spectrum. The crystal structure of IrPYE-Cl confirmed the two-legged piano stool geometry as reported for previous complexes.

2.2.3 Synthesis of compound 8

As we successfully synthesized and characterized IrPYE-Cl, we aimed to next synthesize a variant with a longer carbon-chain between the amide and chloride leaving group (Scheme 8). We hypothesize that its reactivity could differ from IrPYE-Cl when attached to a resin, as the distance to the solid support increases.

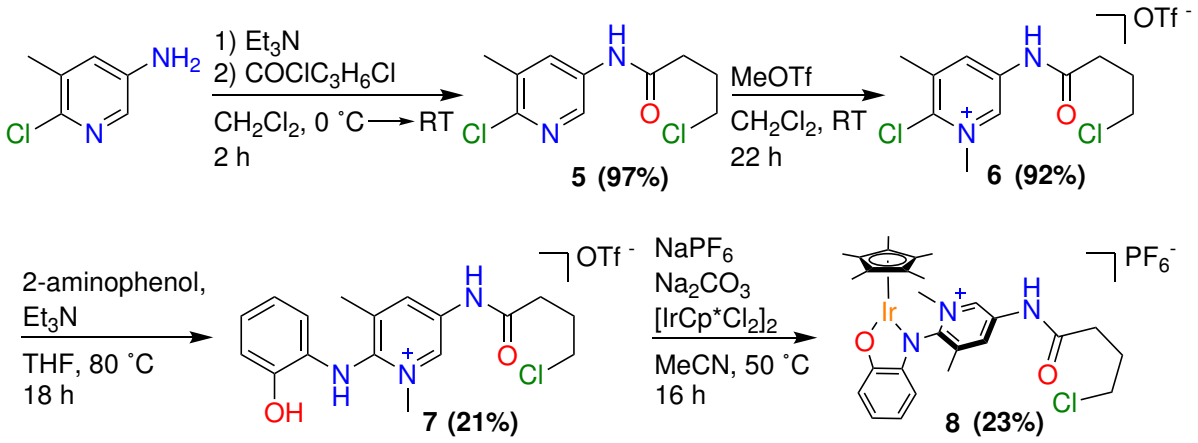

Scheme 8: Synthesis of compound **8**.

We again aimed to mimic established procedures. Hence, 4-chloro-butyryl chloride was used as a substitute for the chloroacetyl chloride used in the synthesis of compound **1**, synthesizing compound **5**. Compound **5** was fully characterized.

We synthesized compound **2** by methylating compound **5** *via* MeOTf. The reaction was followed by ^{1}H NMR spectroscopy and HRMS. The reaction was successful, synthesizing **6**, which was fully characterized.

To synthesize compound **7**, the 2-aminophenol was attached on compound **6** *via* an S_NAr reaction. Over the duration of the reaction, a yellow precipitate formed, similar to the formation of compound **3**. Upon removal of the solvent, and subsequently redissolving the remaining material in $CHCl_3$, a white precipitate formed. This white solid was identified as compound **7** and fully characterized.

The complexation of the ligand to the $[IrCp^*Cl_2]_2$ yielded compound **8**. The conditions for the complexation remained unchanged from the protocol for IrPYE-Cl. The reaction was followed *via* ^{1}H NMR spectroscopy. The signals of the aminophenol-moiety of the ligand underwent a characteristic change during complexation, indicating that the reaction took place. Compound **8** was fully characterized. Similar to IrPYE-Cl, the typical Cp* signal was observed 1.69 ppm. The two methyl signals were observed at 2.10 and 3.97 ppm, while the characteristic aromatic heterocycle signals were observed at 8.50 and 9.41 ppm. Additionally, the three methylene signals were observed at 2.16, 2.71, and 3.72 ppm in the ^{1}H NMR spectrum. Due to time constraints, we could not obtain a crystal X-ray structure.

2.3 Synthesis of a nucleophilic complex

As we synthesized electrophilic complexes, we aimed to also access nucleophilic complexes. As the electrophilic compounds are now readily available, we tried to leverage them to access nucleophilic derivates.

2.3.1 Synthesis of nucleophilic derivates of compound 1

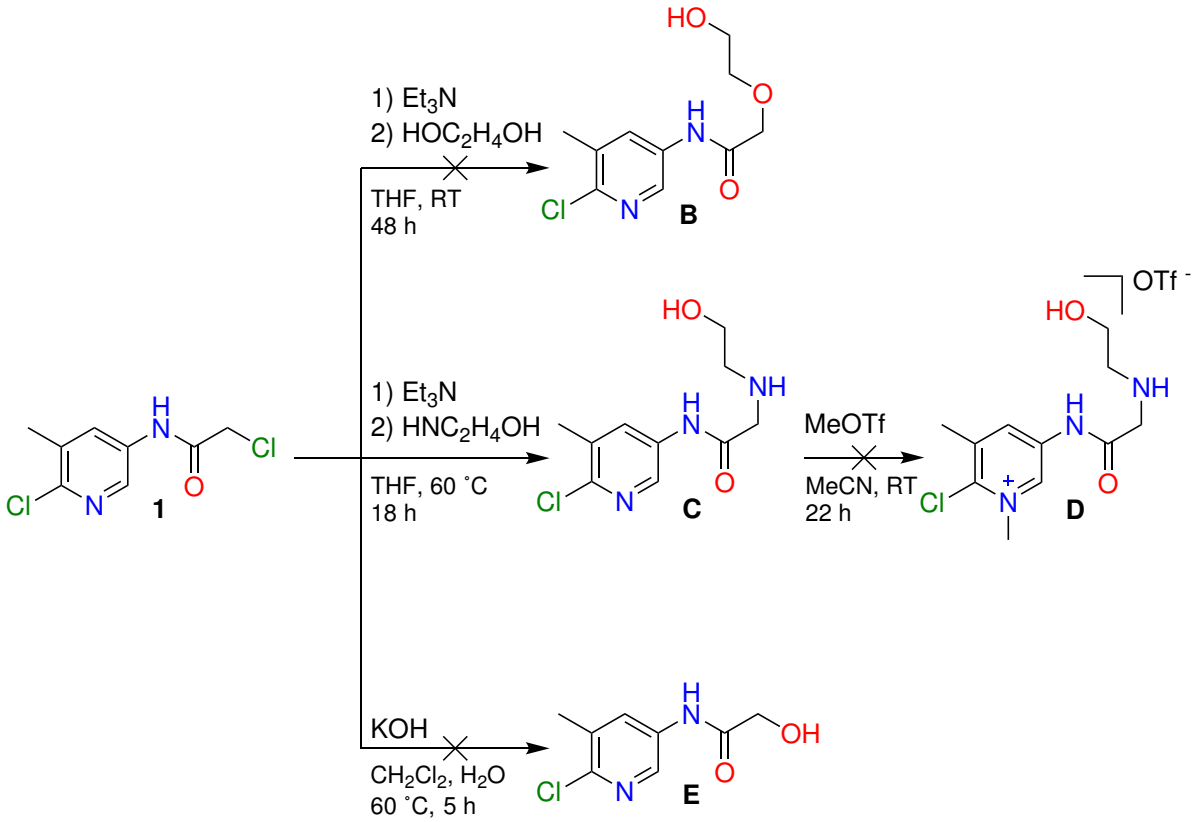

Scheme 9: Synthetic pathways of modified pyridines, using compound **1** as a starting point.

We first attempted to react compound **1** with ethylene glycol. Comparing the ^{1}H NMR of the crude compound **B** in CD_2Cl_2, to the ^{1}H NMR of compound **1** in CD_2Cl_2, the characteristic aromatic signals of compound **1** at 8.26 and 7.91 ppm shifted to 8.22 and 7.99 ppm respectively in the spectrum of compound **B**. While these signals make up the major product of the reaction, minor signals in the aromatic region indicate an incomplete conversion and potential side-products.

In order to minimize side reactions, such as dimerization, we replaced ethylene glycol by ethanolamine, hypothesizing that the two different functional groups of the ethanolamine may allow for a more chemoselective reaction. The resulting compound **C** was purified *via* precipitation out of EtOAc and fully characterized. With compound **C** in hand, we next aimed to introduce the second methyl group at the N-heterocycle *via* MeOTf. However, following the reaction *via* HRMS, three major components were visible in the reaction mixture: The starting material at 244.0848 m/z, the desired compound **D** at 258.1005 m/z, as well as the doubly methylated product at 272.1160 m/z (Figure 2). The second methylation is hypothesized to have taken place at the secondary amine. A separation of the mixture was attempted *via* an AlOx neutral column with EtOAc as an eluent, however no separation of the compounds could be achieved.

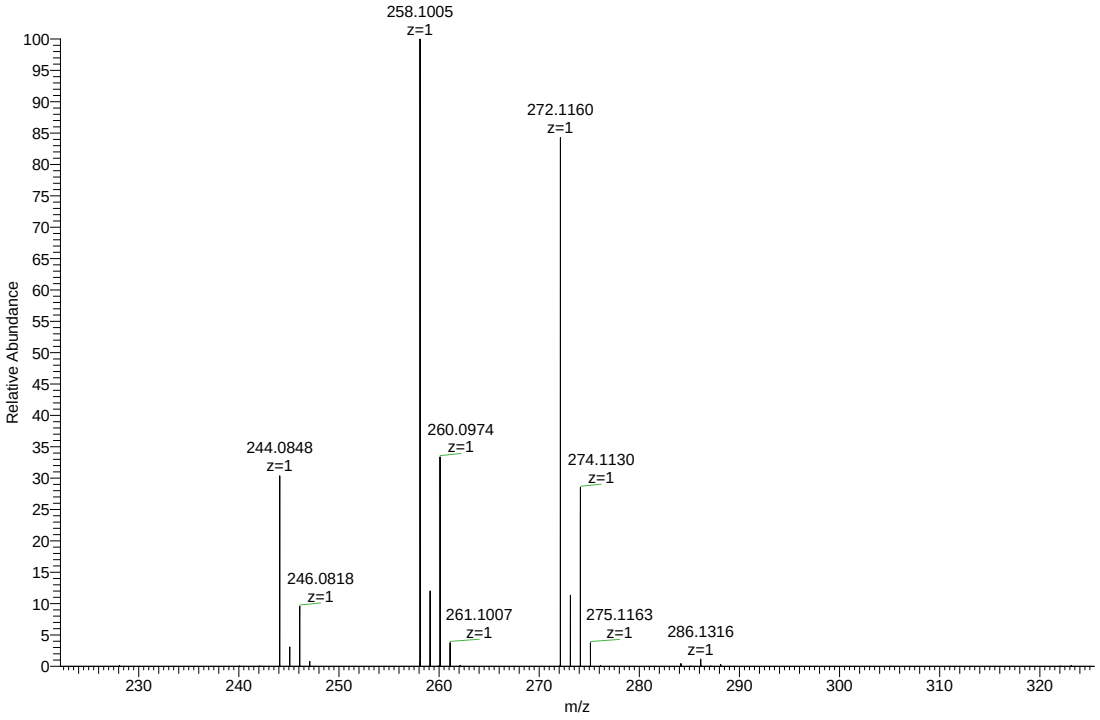

Figure 2: HRMS spectrum of the reaction mixture of compound **D**, containing the starting material (244.0848 m/z), the desired compound **D** (258.1005 m/z), and the doubly methylated product (272.1160 m/z).

Alternatively, we attempted to synthesize compound **E** *via* KOH in a mixture of CH_2Cl_2 and H_2O. The ^1H NMR spectrum suggested the presence of both starting material and the desired product. Although increased temperatures and longer reaction times could potentially push the reaction to completion, we did not pursue it further.

2.3.2 Synthesis of nucleophilic derivates of compounds 2 and 3

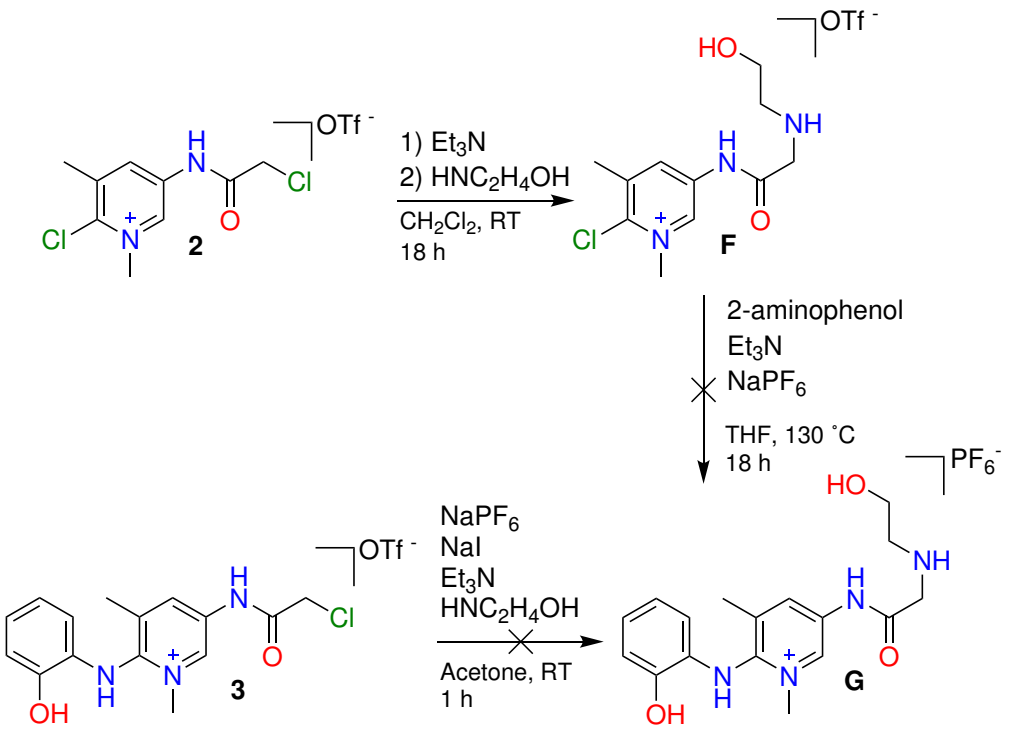

Scheme 10: Synthetic pathways of nucleophilic derivates, using either compound **2** or **3** as a starting point.

As we could not synthesize a nucleophilic derivate of **1**, we shifted the approach, trying to derivatize compound **2** instead. First, ethanolamine was attached on compound **2**. The correct placement of the ethanolamine at the α-carbon protons was confirmed by 2D-NOESY NMR spectroscopy, based on the spatial correlation between the methylene protons at 3.55 ppm and the α-carbon at 4.37 ppm. Additionally, there was a lack of spatial correlation between the methylene protons at 3.55 ppm and either of the methyl group signals at 2.41 or 4.00 ppm. Compound **F** was fully characterized.

We then attempted to synthesize compound **G**, *via* an S_NAr reaction of 2-aminophenol on compound **F**. The exchange of the counteranion *via* $NaPF_6$ was done to increase the solubility of compound **F** in the THF used as the solvent during the reaction. However, no conversion into the product could be seen in the ^1H NMR spectrum, despite the elevated temperature of 130 °C provided for the reaction. The characteristic aromatic signals at 8.24 and 7.80 ppm show no shift during the reaction. The 2-aminophenol signals at 6.34 and 6.19 ppm also do not shift. Additional 2-aminophenol was added to the NMR tube to ensure that the signals indeed belong to free 2-aminophenol, suggesting no conversion into the desired compound **G**.

We therefore shifted the approach again, attempting to synthesize compound **G** through a Finkelstein reaction from compound **3**. However, all attempts to characterize the crude product *via* ^1H NMR spectroscopy were unsuccessful due to signal overlap and complexity of the spectrum. It was therefore not further pursued.

2.3.3 Synthesis of nucleophilic derivates of compound 4

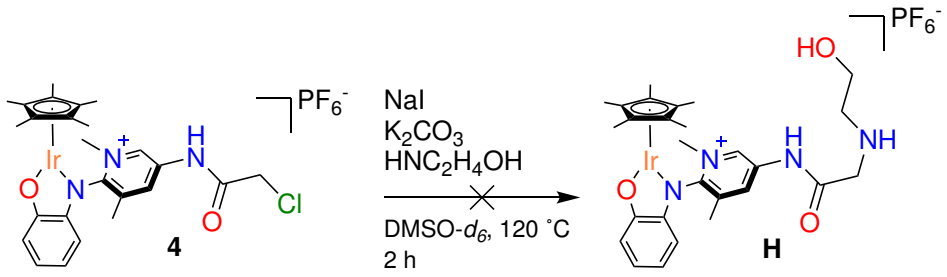

Scheme 11: Synthetic pathway of a nucleophilic derivative, using compound **4** as a starting point.

In a last attempt at creating a nucleophilic variant of the complex, we tried the addition of ethanolamine *via* a Finkelstein reaction in DMSO-d_6 on compound **4**. The NaCl from the Finkelstein reaction has a low solubility in the DMSO-d_6 and should precipitate upon formation. This is supposed to push the equilibrium of the reaction towards the iodinated complex, allowing an easier S_N2 reaction of the ethanolamine on the α−Cl. To work up compound **H**, CH_2Cl_2 was added to the crude. It was then layered with Et_2O and cooled to -20 °C in the freezer, attempting to precipitate the product. However, the DMSO-d_6 froze at these low temperatures, partially crystallizing in solution. The now solid DMSO-d_6 and the CH_2Cl_2-Et_2O solvent mixture were separated. Both of them were analysed *via* ^{1}H NMR spectroscopy, no characteristic aromatic signals could be attributed to any major product, and the synthesis of a nucleophilic complex was not further pursued.

2.4 Resin preparation

We aimed to functionalize four different resins to contain amine groups, to covalently immobilize the previously discussed IrPYE-Cl. Different resins were used, because the material of the solid support can greatly influence the reactivity of the immobilized catalyst. We aimed to test the differences between the solid supports. The different hydrophobicities and pore sizes of the resins may lead to different interactions with the substrates, influencing the final activity. The amount of active groups on the resin surface differed greatly between resins, likely leading to different complex loading. Therefore, in order to control the stoichiometry of the reaction, we measured the amount of functional groups on the resin, if not provided by the manufacturer.

Resin	Type	Epoxy groups (µmol/g dry resin)	Amine groups (µmol/g dry resin)
Rapid Run Agarose	Agarose	950	950
HFA403/S	Methacrylate	104.2	104.2
S2200	Silica	n.a.	129.8
Silicycle	Silica	n.a.	1710

Table 1: The type, as well as the amount of epoxy or amine groups of the four resins employed in this work.

We first functionalized an agarose resin to contain an epoxy group. It was then dried on a Lyophylizer, where it lost 92% of its weight after drying. The epoxy group density was measured to be 84 µmol/g wet resin, and 950 µmol/g dry resin. These findings correlate with each other in relation to the weight the resin lost during the drying process. We further functionalized the dried agarose resin to contain an amine group, yielding the Amino-Agarose-Resin. Given the extended reaction time, we assumed that all available epoxy groups had reacted with the ethylene diamine. Therefore, the amine group density was estimated at 84 µmol/g wet Amino-Agarose-Resin, and 950 µmol/g dry Amino-Agarose-Resin.

We modified HFA403/S resin, pre-functionalized with epoxy groups, to contain amine groups, yielding the Amino-Methacrylate-Resin. It was then lyophylized, resulting in a 66% weight loss. As the manufacturer provides the epoxy group density with 35 µmol/g wet resin, the material was weighed before and after drying to calculate the functional group density in the dry state, resulting in 104.2 µmol/g dry resin. Similarly to the Amino-Agarose-Resin, we assumed complete conversion of the epoxy groups by ethylene diamine. Therefore, the amine group density was estimated at 104.2 µmol/g dry Amino-Methacrylate-Resin.

Furthermore, SiliaBond Amine resin (Silicycle) was bought. The manufacturer provides the amine group density with 1.71 mmol/g dry resin. This is significantly higher than any other resin employed in this work.

2.4.1 Amino-Silica amine group determination

Next, we functionalized Sipernat® 2200-PC Silica microbeads (S2200) to contain amine groups. The protocol was adapted from Benítez-Mateos et al., who used 3-glycidyloxypropyl trimethoxysilane to functionalize S2200 to contain epoxy groups.[59] This yielded the Amino-Silica-Resin. The amine group density was measured with 2,4,6-trinitrobenzene sulfonic acid (TNBSA). TNBSA reacts with free amines to form an equilibrium between the Mesenheimer anion and trinitrophenylamine (Scheme 12).[60] The Mesenheimer anion has its absorption maximum at 420 nm, while trinitrophenylamine has its absorption maximum at 340 nm.

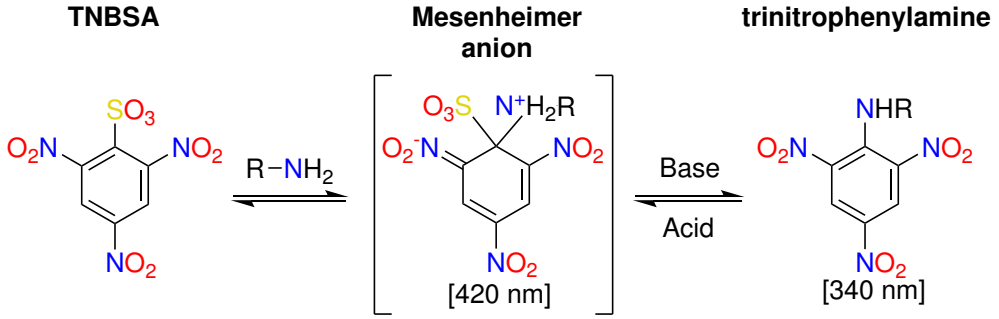

Scheme 12: The formation of the Mesenheimer anion (middle) from TNBSA (left), as well as its acid-base mediated equilibrium with trinitrophenylamine (right).

We initially used a solution of TNBSA in H_2O as supplied by the manufacturer. However, we observed a yellow discolouration of the normally colourless solution. ^{1}H NMR analysis of the bottle's contents suggested the presence of a decomposition product. Two sets of signals were observed in the aromatic region: a major singlet (8.86 ppm) integrating to 1, and a smaller singlet (8.92 ppm) integrating to 0.25. This indicated that approximately 25% of the TNBSA had hydrolysed to picric acid. Picric acid exhibits an absorption maximum at 352 nm, which can interfere with attempts at an accurate quantification. We decided to switch to a solution of TNBSA in DMF to minimize the formation of picric acid during longer storage time. The new solution was used to create a calibration curve in MeCN, with added ethanolamine and an excess of HCl (Figure 3). MeCN was chosen as the solvent, as its UV cutoff at 190 nm will not interfere with the measurement at 420 nm. The ethanolamine reacts with the TNBSA, forming the equilibrium between the Mesenheimer anion and trinitrophenylamine, while the added HCl will shift the equilibrium towards the Mesenheimer anion (Scheme 12, middle).[60]

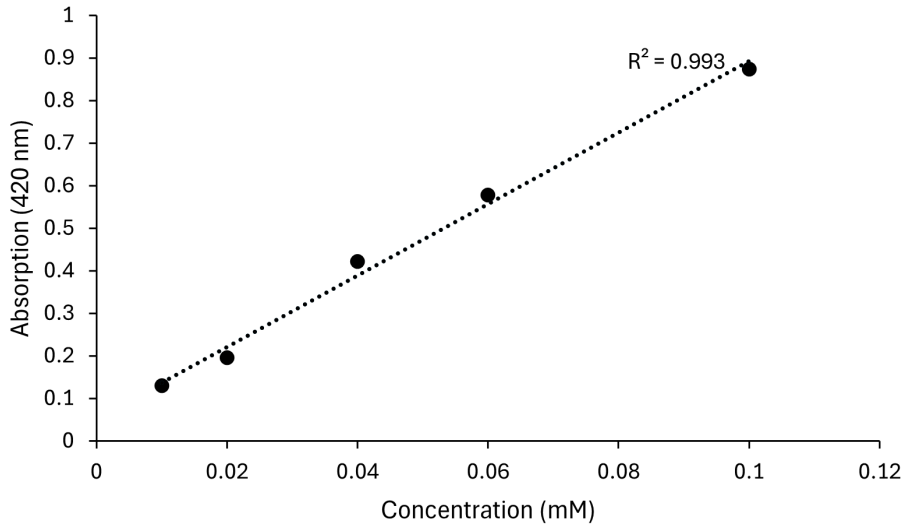

Figure 3: A calibration curve of TNBSA, ethanolamine, and HCl in MeCN, for the determination of amine functional groups on the Amino-Silica-Resin.

When the TNBSA solution was added to the Amino-Silica-Resin, it immediately showed a bright orange discolouration. By calculating the leftover concentration of TNBSA, we could deduce the amount of TNBSA that had reacted with the amine groups and, by extension, determine the amine group density. The amount of resin that was weighed out allows for the calculation of total amine groups, i.e. 129.8 µmol/g dry Amino-Silica-Resin.

2.5 IrPYE-Cl immobilization on resins

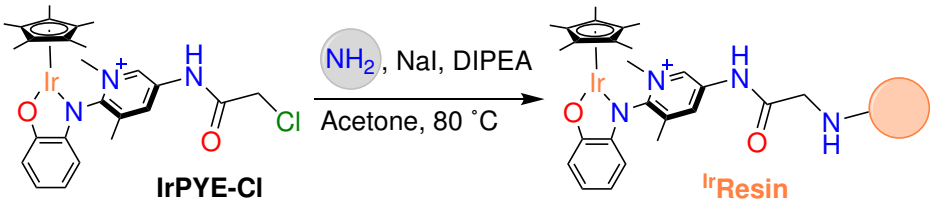

Scheme 13: The scheme of the immobilization of IrPYE-Cl on an Amino-Resin.

As we quantified the amine group densities of the different resins, we could now immobilize the IrPYE-Cl on the different resins *via* a Finkelstein reaction. All reagents had to be water-free, as any H_2O present could potentially lead to the hydrolysis of the $\alpha-Cl$ needed for covalent attachment. The total amount of amine groups on the resin used equalled 1 equivalent.

During the synthesis, we already noticed, that nucleophilic attacks on the $\alpha-Cl$ is unfavoured. We therefore used 2 eq. of IrPYE-Cl, and an excess of NaI and N,N-Diisopropylethylamine (DIPEA) in acetone, at 80 °C (Scheme 13). We assumed that any potential side reactions or complex degradation could be ignored, as these products will likely not be immobilized on the resin, and will be washed out during the workup of the ^{Ir}Resins.

Washing the functionalized resins with acetone, MeCN, and subsequently H_2O, yielded the ^{Ir}Agarose, ^{Ir}Methacrylate, ^{Ir}Silica, and ^{Ir}Silicycle, all were discoloured orange.

2.6 Immobilized IrPYE-Cl quantification methods

2.6.1 Quantification *via* KCN

To quantify the amount of iridium bound to the resin, we hypothesized that treatment with a strongly coordinating ligand could displace the metal centre by competing with the original ligand. The released iridium complex could then potentially be quantified by UV-Vis spectroscopy. To test this hypothesis, the resin was treated with a solution of KCN. Upon addition, the resin rapidly turned purple, indicating a change in the coordination environment around the metal centre. Despite filtration and rigorous washing, the purple discolouration remained on the resin. This observation suggests that cyanide ligands coordinated to the iridium centre without fully displacing the PYE ligand and that the release of the metal complex into solution was not fully achieved. Therefore, this method can not be used for an accurate quantification of the immobilized catalyst.

2.6.2 Quantification *via* weighing

We aimed to quantify the amount of immobilized complex per gram of dry resin. The simplest method to achieve this is to weigh the resin before immobilization of the catalyst, and after the immobilization.

We used this method for the Amino-Agarose-Resin, which was used for the IrPYE-Cl immobilization. 50 mg of dry resin were used, and after working up the resin and drying it, the ^{Ir}Agarose weighed 58 mg. Therefore, 137.9 mg IrPYE-Cl have been immobilized on 1 gram of ^{Ir}Agarose. While this method may work for quick assessments, we need better ones for more precise quantifications.

2.6.3 Quantification *via* UV-Vis

We hypothesized to achieve a more accurate quantification with the help of UV-Vis measurements of the supernatant during the immobilization. By measuring the leftover IrPYE-Cl in solution, we can deduce the amount of IrPYE-Cl immobilized on the ^{Ir}Resin. This approach is similar to the one usually employed to measure the amount of immobilized enzyme, where the leftover enzyme concentration in the supernatant is also used to indirectly calculate the amount of immobilized enzyme. To ensure that the other compounds during the immobilization do not interfere with our UV-Vis measurement, we recorded separate spectra of IrPYE-Cl (0.2 mM), NaI (0.4 mM), and DIPEA (0.4 mM), in a solution of equal parts H_2O, acetone, and MeCN (Figure 4).

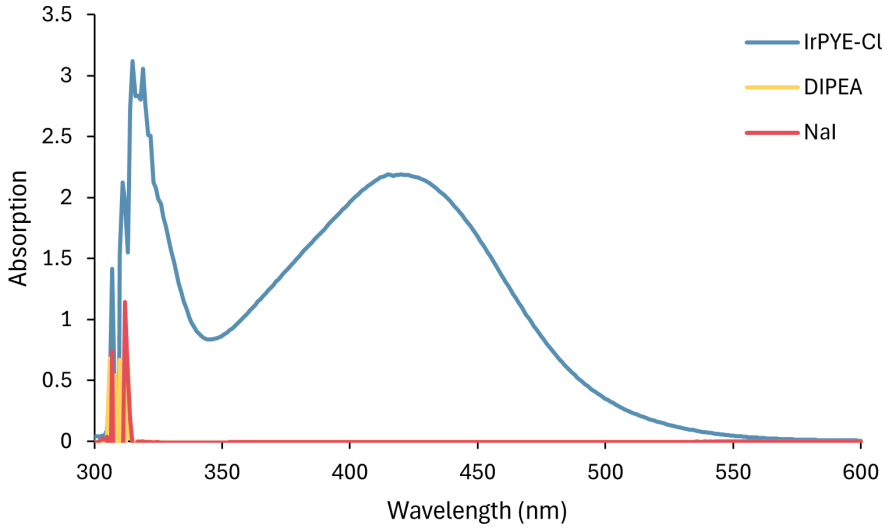

Figure 4: The absorption spectra of IrPYE-Cl, DIPEA, or NaI in a solution of equal parts H_2O, acetone, and MeCN.

The only compound absorbing in the visible spectrum is the IrPYE-Cl, no interference is observed from the DIPEA or NaI.

Full spectra were recorded to determine the absorption maximum of the complex in solution with all compounds present (Figure 5).

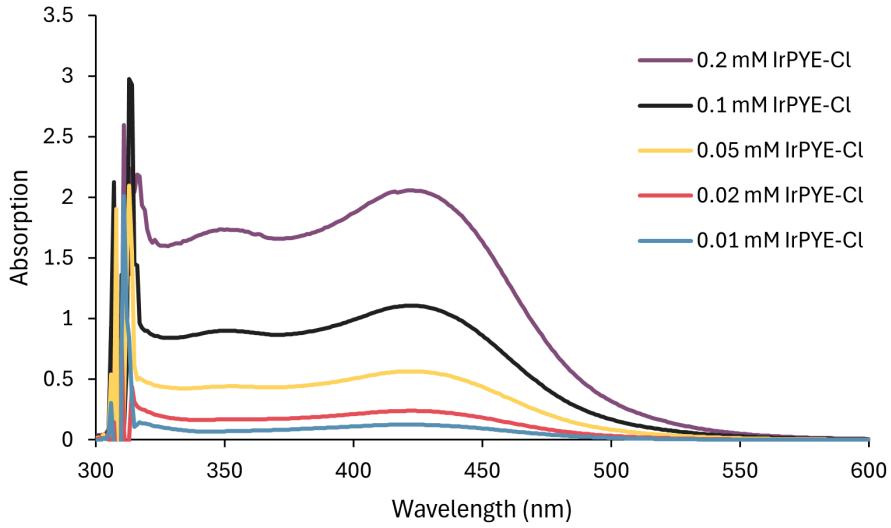

Figure 5: The full spectra of different concentrations of IrPYE-Cl, DIPEA, and NaI, in a solution of equal parts of H_2O, acetone, and MeCN

The absorption maximum of the solution was recorded to be at 423 nm, and a calibration curve was plotted from the obtained data (Figure 6).

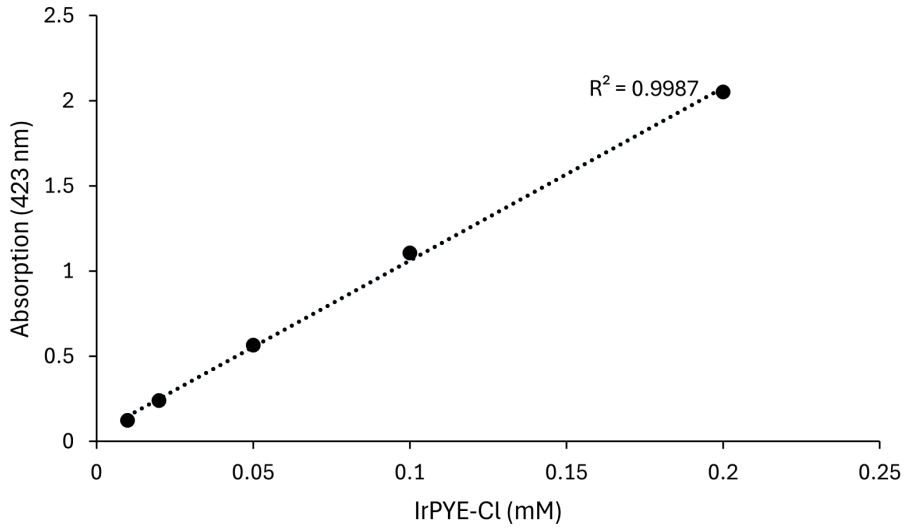

Figure 6: The calibration curve of IrPYE-Cl for UV-Vis quantification of ^{Ir}Resins

We calculated the average molar extinction coefficient, $\varepsilon = \frac{E}{cd}$, to be 11435.2 L mol^{-1} cm^{-1}. The amount of unreacted IrPYE-Cl was measured, and by subtracting it from the total amount offered, the quantity of immobilized catalyst was deduced.

Amino-Methacrylate-Resin was used for the IrPYE-Cl immobilization. The original IrPYE-Cl concentration of the mixture was calculated to be 8.47 mM. After 1 h, the average absorption at 423 nm was measured to be 1.655. With the molar extinction coefficient and the dilution factor, we can calculate the IrPYE-Cl concentration of the solution:

$$c = \frac{E}{\varepsilon d} * 60 = 8.4 \text{ mM}.$$

The difference of 0.07 mM suggested, that 1.3 mg IrPYE-Cl have been immobilized on 1 gram of ^{Ir}Methacrylate. After 5 h, the average absorption at 423 nm was measured to be 1.775, which equaled a concentration of 9.3 mM. This was higher than the original concentration. This could be the consequence of the acetone evaporating during the reaction. The septum in the microwave-vial lid had to be pierced to take the 1 h sample. As the immobilization is performed at 80 °C, the gas pressure could be high enough for the acetone to evaporate through these small breaches in the septum.

Next, the Amino-Silica-Resin was used for the IrPYE-Cl immobilization. After 2 h, The average absorption at 423 nm was measured to be 1.24. With an expected concentration of 7.96 mM, we can calculate that 36.9 mg IrPYE-Cl have been immobilized on 1 gram of ^{Ir}Silica.

Next, the Silicycle resin was used for the IrPYE-Cl immobilization. After 2 h, the average absorption at 423 nm was measured to be 1.39. With an expected concentration of 8.52 mM, we can calculate that 400 mg IrPYE-Cl have been immobilized on 1 gram of ^{Ir}Silicycle. This is the highest value of immobilized catalyst of all the resins (Table 2).

^{Ir}Resin	Immobilized complex (mg/g dry resin)	Immobilization yield (%)
^{Ir}Methacrylate	1.3	0.8
^{Ir}Silica	36.9	18.3
^{Ir}Silicycle	400	15.1

Table 2: The amount of immobilized complex on ^{Ir}Agarose (quantified *via* weighing), ^{Ir}Methacrylate (quantified *via* UV-Vis), ^{Ir}Silica (quantified *via* UV-Vis), ^{Ir}Silicycle (quantified *via* UV-Vis). All ^{Ir}Resins were incubated with 2 eq. of IrPYE-Cl

The measurements of the ^{Ir}Methacrylate showed, that this method is unreliable when wanting to take multiple samples over several time-points, due to the errors introduced by the manipulations.

2.6.4 Quantification *via* ICP-MS

We hypothesized to achieve more precise and reliable results with inductively coupled plasma mass spectrometry (ICP-MS) analysis. This method allows for the detection of iridium concentrations in the µg/L range.

By using harsh aqua regia extractions on the ^{Ir}Resins to create the sample solutions, we aimed to ensure higher accuracy and reproducibility.

In first screenings, we took samples of ^{Ir}Resins, all incubated with 2 eq. of IrPYE-Cl each. Multiple subsequent extractions were performed on the same sample.

^{Ir}Resin	^{Ir}Resin used (mg)	1st extraction (mg/g dry resin)	2nd extraction (mg/g dry resin)	residual iridium after 1st extraction (%)
^{Ir}Agarose	4.9	18.26	n.a.	n.a.
^{Ir}Methacrylate	4.0	1.18	0.13	9.92
^{Ir}Silica	17.8	39.08	5.05	11.44
^{Ir}Silicycle	4.4	287.53	1.62	0.56

Table 3: The amount of immobilized complex on ^{Ir}Agarose (no grinding), ^{Ir}Methacrylate (no grinding), ^{Ir}Silica (grinding *via* a stir-bar), ^{Ir}Silicycle (grinding *via* a stir-bar). All ^{Ir}Resins were incubated with 2 eq. of IrPYE-Cl.

Both the ^{Ir}Methacrylate and ^{Ir}Silica showed high residual amounts of iridium in their 2nd extraction compared to their 1st (Table 3). We performed additional measurements, after preparing new batches of ^{Ir}Resins. Even higher amounts of residual iridium were measured. In an ^{Ir}Methacrylate sample, the 1st extraction showed 0.56 mg/g dry resin, while the 2nd extraction showed 4.05 mg/g dry resin. This was puzzling as the 2nd extraction had an even higher dilution factor than the 1st.

In trying to circumvent this, we used even harsher conditions during the extractions (60 °C during incubation with aqua regia). This way, most iridium should be extracted with the first wash and only residual iridium should be measured in subsequent extractions (Table 4).

^{Ir}Methacrylate Batch	^{Ir}Resin used (mg)	1st extraction (mg/g dry resin)	2nd extraction (mg/g dry resin)	3rd extraction (mg/g dry resin)
1	5.6	0.96	0.15	n.a
2	4.3	0.99	0.09	0.0

Table 4: The amount of immobilized complex on ^{Ir}Methacrylate batches (grinding *via* a stir-bar at 60 °C). ^{Ir}Methacrylate was incubated with 0.5 eq. of IrPYE-Cl.

Even with higher temperatures, 13.5% residual iridium in a 2nd extraction was not satisfactory, more extractions seemed to be necessary (Table 4, entry 1). Therefore, 4 subsequent extractions were performed. This time, the 3rd extraction showed values no higher than the

submitted aqua regia blank. This value, stemming from a duplicate, suggested a successful quantification with the ICP-MS measurements, and the same workflow was therefore adapted to the ^{Ir}Silicycle. As we observed in multiple cases, due to the low concentrations and high dilutions, this method is highly susceptible to iridium contamination.

2.6.5 Comparisons between quantification methods

We compared the values from the weighing or UV-Vis measurements, and the ICP-MS measurements. Except for the ^{Ir}Methacrylate, all other measurements differed drastically, with the ^{Ir}Agarose showing the highest difference, suggesting that the weighing method is likely unreliable (Table 5).

^{Ir}Resin	weighing / UV-Vis (2 eq.) (mg/g dry resin)	ICP-MS (2 eq.) (mg/g dry resin)	ICP-MS (0.5 eq.) (mg/g dry resin)
^{Ir}Agarose	137.9	18.26	n.a.
^{Ir}Methacrylate	1.3	1.31	0.99±0.016
^{Ir}Silica	36.9	44.13	n.a.
^{Ir}Silicycle	400	289.15	48.84±1.06

Table 5: The amount of immobilized complex on ^{Ir}Resins, measured either *via* weighing/UV-Vis or ICP-MS. All ^{Ir}Resins were incubated with either 0.5 or 2 eq. of IrPYE-Cl.

The ICP-MS quantification proved to be the most reliable and precise method of all discussed, and can potentially also be applied to many other heterogeneous TM-catalyst systems for accurate quantification of immobilized catalyst. Not relying on small amounts of volatile solvents and many subsequent dilutions, compared to the UV/VIS quantification, is likely why the recorded values differed. In conclusion, if no contaminated instruments are used while preparing the samples, the ICP-MS workflow is the most reliable and accurate of all the quantification methods presented.

Since we observed that only up to 18% of the total provided IrPYE-Cl was immobilized in the UV-Vis measurements, we decided to lower the total amount of offered catalyst to 0.5 eq., to avoid wasting precious iridium. All other compounds were kept at their original equivalents.

2.7 Resin Microscopy

The morphology of the different resins can have an influence on their ability to be functionalized, as well as their potential catalytic activity. We therefore inspected all resins under a Nikon "Eclipse TS2 inverted routine microscope" (Figure 7).

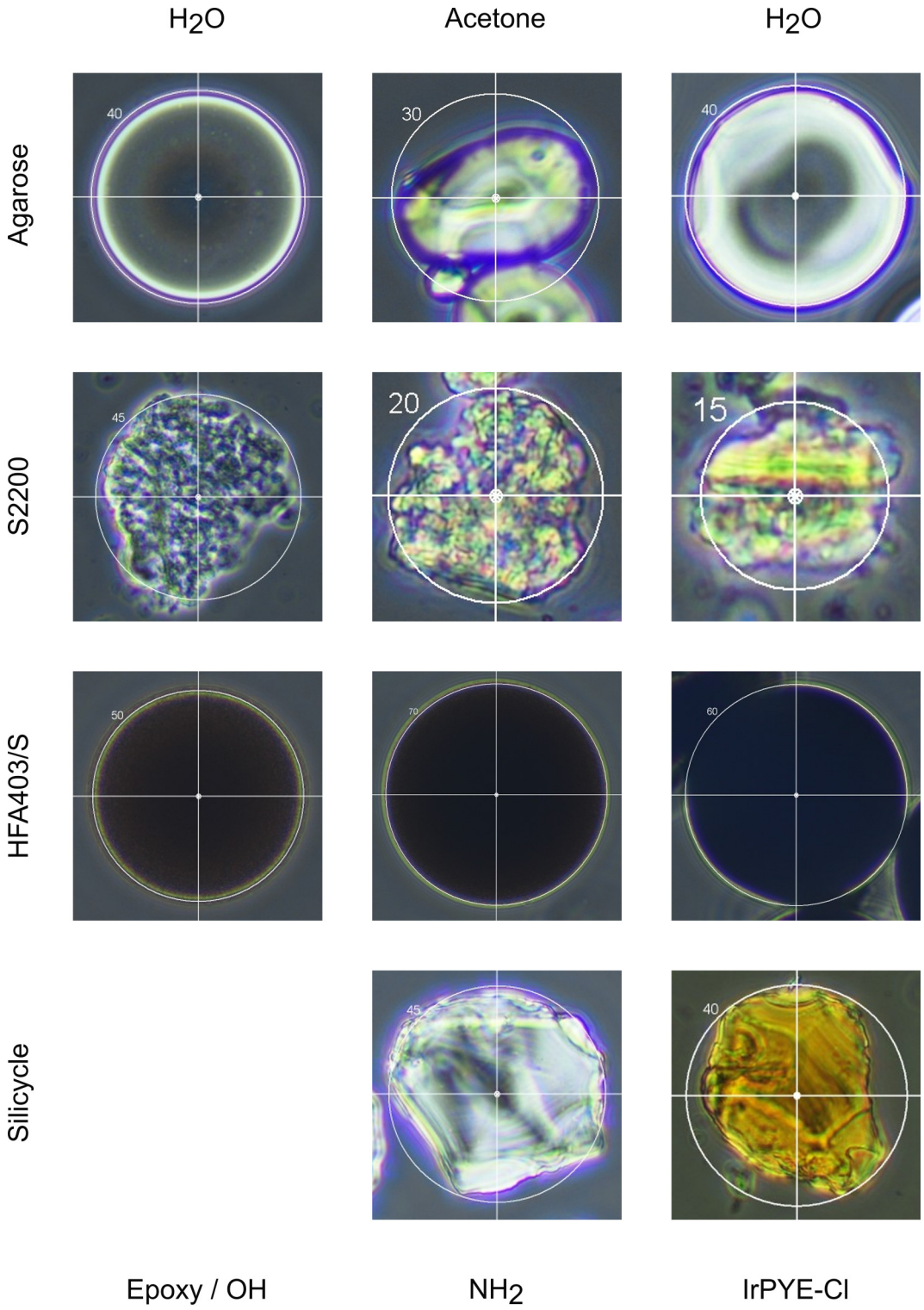

Figure 7: The different resins (left), their functionalization (bottom), in different solvents (top).

The solvents were chosen, so that they match the ones employed in the next step of their treatment. Thus, the epoxy/OH functionalized resins used H_2O as the solvent, as this is the solvent used to further functionalize them to the amine. The amine functionalized resins used Acetone as the solvent, as this is the solvent used during the immobilization of the IrPYE-Cl on the resins. The ^{Ir}Resins used H_2O as the solvent, as this is the solvent used in the NADH regeneration reactions, as well as during the combined assays with the enzymes.

All epoxy/OH functionalized resins showed an expected morphology, with the Agarose and HFA403/S resins being spherical, while the S2200 consisted of irregularly shaped particles. All resins were dried after the amine functionalization.

The Amine-Agarose-Resin showed a clear change in morphology due to this drying *via* the Lyophylizer. Even after the immobilization of the complex and reswelling the ^{Ir}Agarose in H_2O, it did not fully regain its original morphology. This could possibly influence its ability to properly catalyse reactions, as it is unclear what exactly happens on the surface of the resin.

The Amine-Silica-Resin still consisted of irregularly shaped particles, which seemed to shrink further in size in the subsequent functionalization step. ^{Ir}Silica was composed of many small particles, it is not yet clear if it can be employed, as if the particles become too small, they could wash through the filters of the syringes employed.

The Amine-Methacrylate-Resin showed no changes in morphology.

The Silicycle resin also showed no clear changes in morphology. The advantage of this resin are therefore two-fold: It does not become so small to wash through the employed filters in the syringes, and it has the highest amount of catalyst immobilized according to the ICP-MS measurements.

2.8 Aldehyde reduction *via* ^{Ir}Resins

The reduction of 4-fluorobenzaldehyde *via* IrPYE has previously been reported by Lentz et al.[57] This allowed us to compare the activity of our ^{Ir}Resins (Scheme 14) to the state of the art IrPYE complex.

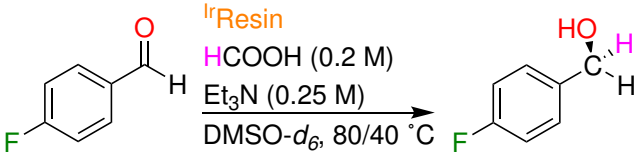

Scheme 14: The scheme of the catalytic reduction of 4-fluorobenzaldehyde *via* an ^{Ir}Resin.

^{Ir}Resin	Temperature (°C)	Substrate (mM)	Catalyst loading (mol%)	TON
^{Ir}Agarose	80	160	1	<1
^{Ir}Silica	80	160	2.3	44
^{Ir}Methacrylate	40	16	1	82
^{Ir}Silicycle	40	160	1	89

Table 6: The temperature, substrate concentration, catalyst loading, and TON of the different ^{Ir}Resins, during the catalytic reduction of 4-fluorobenzaldehyde.

We first employed ^{Ir}Agarose with a catalyst loading of 1 mol% immobilized complex (determined *via* weighing). For the analysis, the product signal at 7.30 ppm, originating from the ortho-protons, and the substrate signal at 7.44, originating from the ortho-protons, were used. Despite the reaction being run for 72 h, only traces of the product were seen in the ^{1}H NMR spectrum. We hypothesized, that the low activity of the resin towards the substrate could be due to changes in the resin morphology upon functionalization with the metal complex. It showed clear deformation in the microscopy, which could have influenced the activity.

Next, we employed ^{Ir}Silica with a catalyst loading of 2.3 mol% immobilized complex (determined *via* ICP-MS). This number was calculated after performing the reaction, as the ICP-MS quantification method has not yet been established when running this tentative reaction. After 2 h, full conversion was observed in the ^{1}H NMR spectrum. To sample the reaction, the resin was filtered, and the filtrate analysed. During this process, we observed that a significant fraction of the resin passed through the filter membrane, resulting in catalyst loss. This behaviour is most likely due to the small particle size of the resin. As previously observed by microscopy imaging, the resin functionalization process significantly disrupted the bead morphology, leading to the formation of smaller particles. The bead's degradation explains the catalyst loss during filtration and suggests an overall instability of the material. Although ^{Ir}Silica efficiently catalysed the reaction, these limitations make its reuse unattractive.

We then probed ^{Ir}Methacrylate with a catalyst loading of 1 mol% immobilized complex (determined *via* ICP-MS) (Figure 8). As the amount of immobilized catalyst per gram of dry ^{Ir}Methacrylate was very low (1.3 mg), we would need to employ large amounts of resin. This

would probably lead to worse mixing of the solution and resin, and more surface-to-surface contact. We opted to instead lower the concentration of the substrate 10-fold. While this can have an influence on the reaction rate, using large amounts of ^{Ir}Methacrylate was unsustainable.

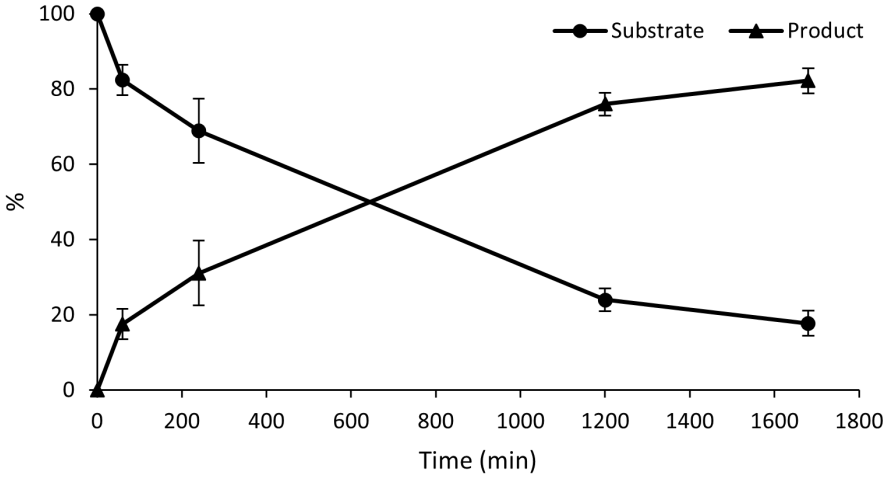

Figure 8: The amount of substrate and product of the aldehyde reduction *via* ^{Ir}Methacrylate over time. The reaction was performed in a duplicate and followed by ^{1}H NMR spectroscopy.

Washing the resin after the reaction with additional DMSO-d_6 showed that both the product and substrate were trapped in the resin. It could be that the substrate and product non-covalently interacted with the hydrophobic surface of the resin. Another explanation could lie in the higher amounts of ^{Ir}Methacrylate needed to reach 1 mol%, which could in turn have held back some of the reaction solution. It could be shown that the ^{Ir}Methacrylate catalyses the reaction and could possibly be employed for NADH regeneration, as it does not wash through the filter.

The last resin we tested was the ^{Ir}Silicycle with a catalyst loading of 1 mol% immobilized complex (determined *via* ICP-MS) (Figure 9). Due to a higher amount of immobilized catalyst, compared to the ^{Ir}Methacrylate, only little ^{Ir}Silicycle had to be employed in comparison. Contrary to the ^{Ir}Methacrylate, neither substrate nor product were trapped in the resin. It remains unclear if this is due to the change in surface-interactions or due to the lower total amount of resin employed. The catalysis with ^{Ir}Silicycle was successful, and reliable. The resin could probably be employed for NADH regeneration, as it also does not wash through the filter either.

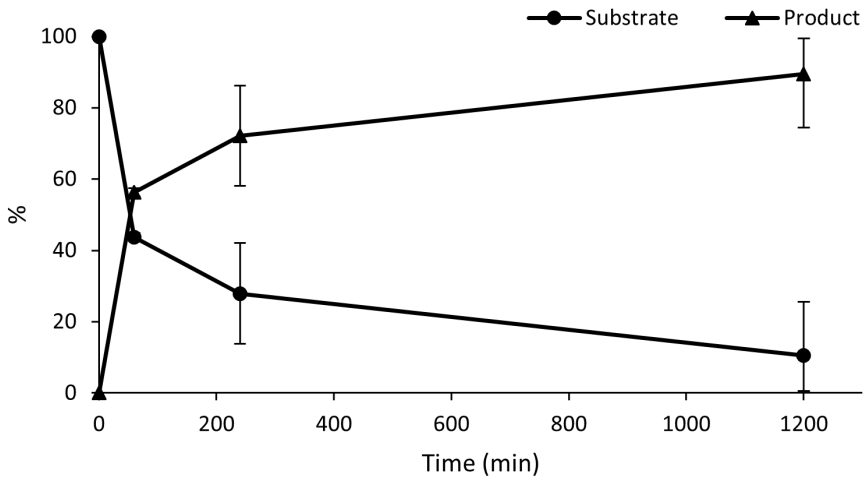

Figure 9: The amount of substrate and product of the aldehyde reduction *via* ^{Ir}Silicycle over time. The reaction was performed in a duplicate and followed by ^{1}H NMR spectroscopy.

While the ^{Ir}Silicycle showed the most promising results, it is still considerably slower compared to the benchmark set by Lentz et al.[57] Both resins that could be employed for the NADH regeneration, ^{Ir}Methacrylate and ^{Ir}Silicycle, catalysed the reaction, albeit considerably slower than IrPYE. The benchmark reaction showed the same reaction reaching >99% yield at a 0.1 mol% catalyst loading at 40 °C after 90 min.

2.9 NADH regeneration *via* ^{Ir}Catalysts

As a next step, we wanted to probe the capability of ^{Ir}Catalysts towards NADH regeneration (Scheme 15). By comparing the results we aimed to find ^{Ir}Resins which we can subsequently use in chemo-enzymatic reactions.

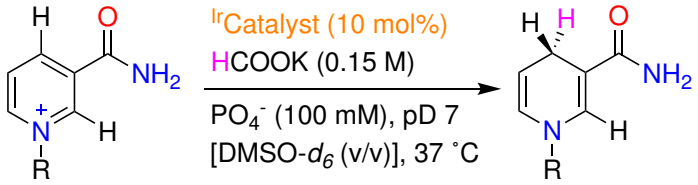

Scheme 15: The scheme of the catalytic regeneration of NADH *via* an ^{Ir}Catalyst.

^{Ir}Catalyst	DMSO-d_6 (% v/v)	Substrate (mM)	Catalyst loading (mol%)	Time (h)	Conversion (%)
IrPYE-Cl	15	10	10	6	3
IrPYE-Cl	15	10	40	4.5	9
^{Ir}Agarose	0	1	100	24	0
^{Ir}Silica	0	10	1	2	45
^{Ir}Methacrylate	0	10	1	18	30
^{Ir}Methacrylate	0	10	1	72	100
^{Ir}Silicycle	0	10	1	2	39
^{Ir}Silicycle	15	10	10	1.25	100
^{Ir}Silicycle	0	10	10	1	96
IrPYE-Acetamide	15	10	10	0.25	100

Table 7: The conversion of NADH regeneration reactions with different ^{Ir}Catalysts, under different conditions, and time-points.

We first probed the activity of IrPYE-Cl towards NADH regeneration. To solubilize it in the aqueous buffer, DMSO-d_6 was utilized. The amount of DMSO-d_6 used was kept at 15% v/v, which is the same amount used in yet unpublished work by Laura Monte. Despite high catalyst loadings of up to 40%, as well as long reaction times, only a low conversion could be measured with IrPYE-Cl. It is highly probable that the α−Cl leads to a lower activity compared to the IrPYE-Acetamide, possibly due to an electron withdrawing effect or solubility issues.

We then employed the ^{Ir}Agarose, despite its low activity in the 4-fluorobenzaldehyde reduction. We tried to circumvent the problem of low reactivity by employing a 100 mol% catalyst loading (determined by weighing) and using only a 1 mM NAD(P)$^+$ concentration. Despite this, no conversion was observed after 24 h.

Next, we probed the ^{Ir}Silica at a 1 mol% catalyst loading (determined by UV-Vis). We saw 45% conversion of the NAD$^+$ after 2 h. A portion of the catalyst was lost during filtration, as reported previously

We next tested the activity of ^{Ir}Methacrylate. As the amount of immobilized catalyst per gram of ^{Ir}Methacrylate was very low compared to the other resins, a large amount of resin was needed for the reaction. At a 1 mol% catalyst loading (determined by UV-Vis), we saw 30% conversion of the NAD^+ after 18 h, and full conversion after 72 h. This is significantly slower than the ^{Ir}Silica. For ^{Ir}Resins to be viable, they must efficiently catalyse the reaction, to minimize the reaction duration. This is because over long reaction times, the enzymes we employed in this work, may cease to function. One solution to this issue would be to employ higher mol% of immobilized catalyst. However, this is not easily possible with the ^{Ir}Methacrylate, because the amount of immobilized catalyst per gram of dry ^{Ir}Methacrylate is comparatively low. The amount of resin needed to reach 10 mol%, for example, would have been so high that it would not have fit in the syringes employed for the reactions. So despite the ^{Ir}Methacrylate catalysing the reaction, it will not be further employed due to this limitation.

Last, we employed the ^{Ir}Silicycle. At a 1 mol% catalyst loading(determined by ICP-MS), we saw 39% conversion, which is slightly lower than with the ^{Ir}Silica. However, the ^{Ir}Silicycle was not lost during filtration, making it preferable over ^{Ir}Silica. As the amount of immobilized catalyst on the ^{Ir}Silicycle was considerably higher than ^{Ir}Methacrylate, we were able to employ a 10 mol% catalyst loading without overloading the syringe. After 1 h, we saw full conversion in the recorded ^{1}H NMR spectrum. We therefore reuse this resin and start cycling with it (Figure 10).

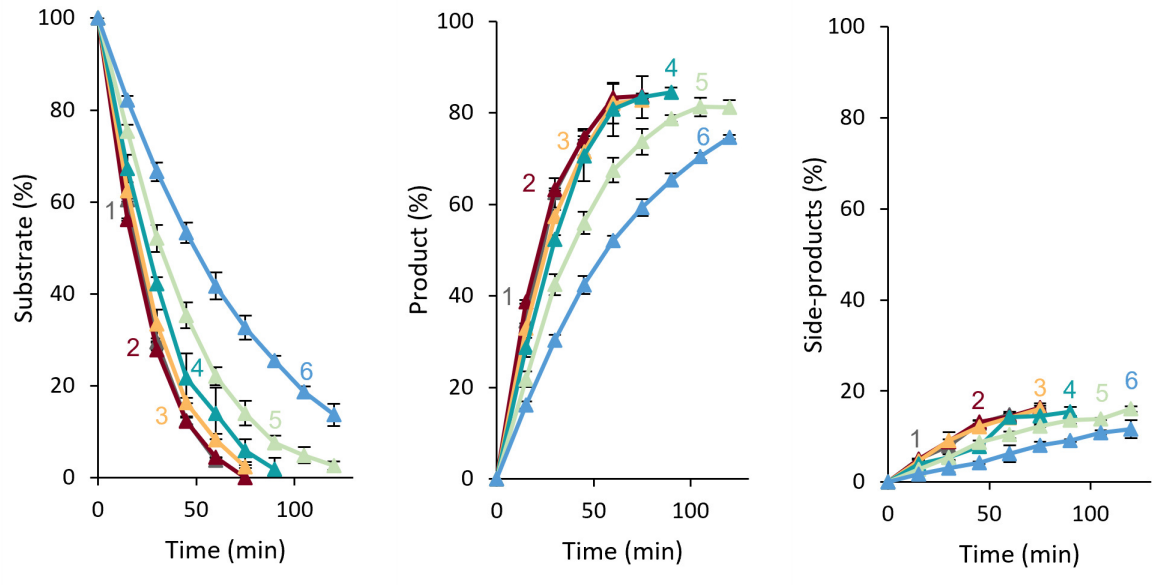

Figure 10: The substrate (left), product (middle), and side-products (right), during the NADH regeneration *via* ^{Ir}Silicycle (10 mol% immobilized catalyst) over time. The resin has been reused over 6 cycles, for a total TON of 58.

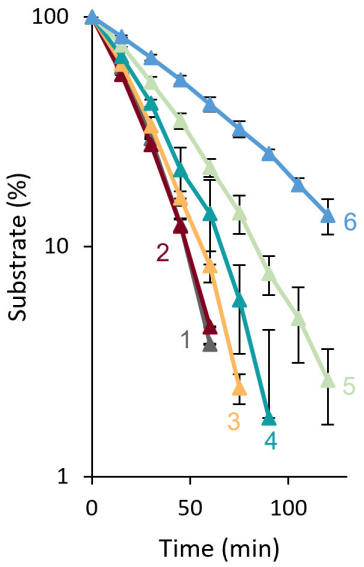

Figure 11: The substrate (on a logarithmic axis) during the NADH regeneration *via* ^{Ir}Silicycle (10 mol% immobilized catalyst) over time. The resin has been reused over 6 cycles, for a total TON of 58.

To more clearly see the loss of activity over the 6 cycles, we changed the Y-axis scale to be logarithmic (Figure 11). The slope for cycle 1 was calculated as -0.024, while the slope for cycle 6 was -0.007. This decrease represents a 3.4-fold loss in activity over the course of the cycles.

The integration of all signals to the internal standard tended to drop slightly over time. Figure 12 shows the sum of all signals (substrate, product, and side-products), during the 6th cycle of the NADH regeneration *via* ^{Ir}Silicycle over time. This is representative for all measurements. These slight changes likely originated from small losses of reaction solution over time, due to the manipulations needed. Therefore, the total amount of reactants, compared to the standard, changed, leading to these differences

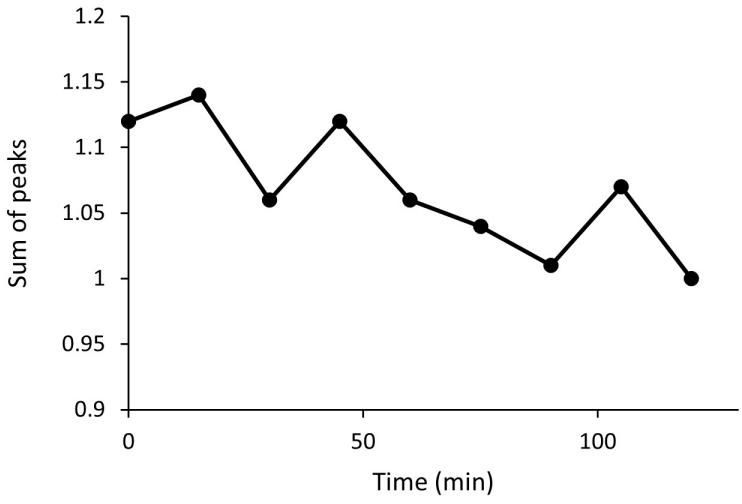

Figure 12: The sum of all signals (substrate, product, and side-products), during the 6th cycle of the NADH regeneration *via* ^{Ir}Silicycle (10 mol% immobilized catalyst) over time.

We observed that the ratio of product to side-products remained consistent at roughly 5.7 across the 6 cycles. However, the side-products will be incompatible with the enzymes employed in this work. If NAD(P)$^+$ is employed sub-stoichiometrically, it will be converted to 85% NAD(P)H, which will immediately be used by the enzyme to catalyse its reaction. However, 15% of the starting NAD(P)$^+$ will be turned into side-products. As we now have a lower amount of total NAD(P)$^+$, we will slowly turn all NAD(P)$^+$ into side-products We can calculate the amount of total NAD(P)H after n full conversions, if we provide a certain amount of starting NAD(P)$^+$, with the help of the following formula:

$$[\text{Total NAD(P)H}] = [\text{starting NAD(P)}^+] \frac{1 - 0.85^n}{1 - 0.85}$$

For example, if we provide 1 µmol NAD(P)$^+$, this will yield a total of 5.4 µmol NAD(P)H over 10 full conversions. The most common unspecific hydrogenation and degradation products recorded in literature, which we hypothesized also made up most of our side products, are shown in scheme 16.[48,49,61]

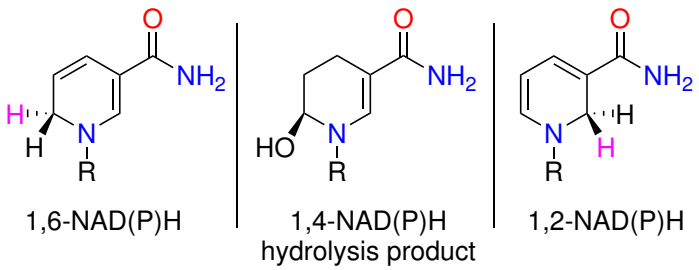

Scheme 16: The most common hydrogenation and degradation products of NAD$^+$.[48,49,61]

In cycle 6, >5% substrate was left after 120 min, so the cycling was stopped. A total TON of 58 was reached. These results are the most reliable obtained with all the ^{Ir}Resins, which is why the ^{Ir}Silicycle was the ^{Ir}Resin used in further assays! When we compare the catalytic activity of the ^{Ir}Silicycle to the IrPYE-Cl, we can also conclude, that the IrPYE-Cl used during the immobilization reaction has undergone a structural change. We hypothesize this reaction to indeed be the covalent immobilization *via* the ligand. If the IrPYE-Cl was to only bind non-covalently to the resin during the immobilization, we would expect similar activities to free IrPYE-Cl during the NADH regeneration.

With the chosen ^{Ir}Resin and conditions in hand, we wanted to compare the activity of the ^{Ir}Silicycle and IrPYE-Acetamide. We also tested the compatibility of the ^{Ir}Silicycle with DMSO-d_6. This is important as there will always be some DMSO present during chemo-enzymatic reactions with enzymes, to solubilize the enzymatic substrate. The addition of DMSO will also allow us to make proper comparisons to the IrPYE-Acetamide, as the DMSO-d_6 is needed to solubilize the complex in the aqueous buffer.

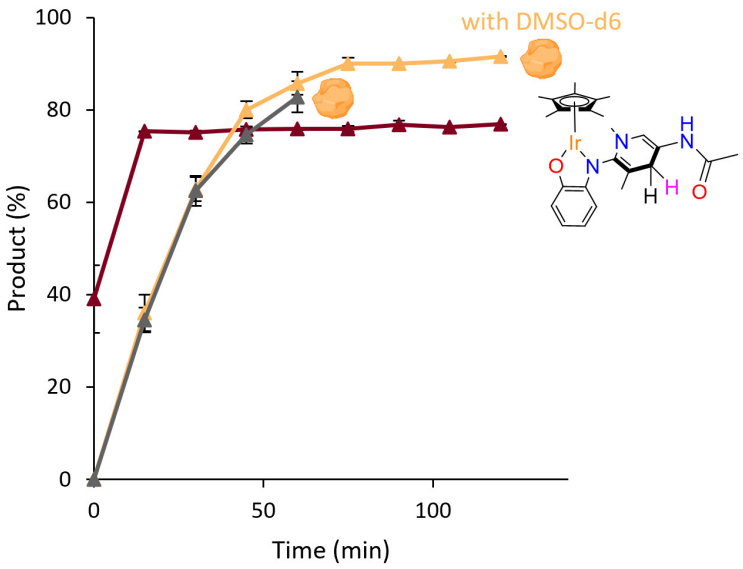

Figure 13: The amount of product during the NADH regeneration *via* IrPYE-Acetamide (red), ^{Ir}Silicycle (grey), and ^{Ir}Silicycle with 15% v/v DMSO-d_6 (yellow) over time. All reactions were performed with 10 mol% (immobilized) catalyst.

While the IrPYE-Acetamide showed full conversion after 15 min, the total yield of NADH was lower than with any of the two ^{Ir}Silicycle conditions. We hypothesized that this is due to the higher reactivity of the IrPYE-Acetamide, potentially leading to more unspecific hydrogenations of the substrate NAD(P)$^+$.

In conclusion, we found that the ^{Ir}Silicycle catalysed the reaction efficiently over 6 cycles. We also observed no loss of the ^{Ir}Silicycle upon filtration. Additionally, higher amounts of immobilized catalyst loading can be employed due to the higher amount of total immobilized complex per gram of dry ^{Ir}Silicycle. Despite the ^{Ir}Silicycle being slower than the IrPYE-Acetamide, it showed a higher yield. Moreover, the addition of the organic solvent DMSO-d_6 during NADH regeneration *via* ^{Ir}Silicycle lead to no relevant changes in catalytic activity. We decided to employ only ^{Ir}Silicycle in all following experiments, due to all these above-mentioned reasons.

2.10 Optimization of enzymatic reactions

As we have found conditions for the NADH regeneration *via* ^{Ir}Silicycle, we next aimed to find suitable conditions for the enzymes. We expressed and purified three different enzymes: "*Mucor circinelloides* old yellow enzyme" (McOYE), "*Halomonas elongata* old yellow enzyme" (HeOYE), and the mutant "*Candida glabrata* ketoreductase F92C F94W" (CgKR1). Similar conditions to the previously optimized NADH regeneration experiment were employed to ensure compatibility between the two systems.

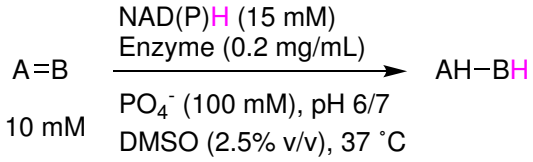

Scheme 17: The scheme of the enzymatic control reaction with stoichiometric amounts of NAD(P)H, an enantioselective reduction of a substrate *via* an NAD(P)H dependant enzyme.

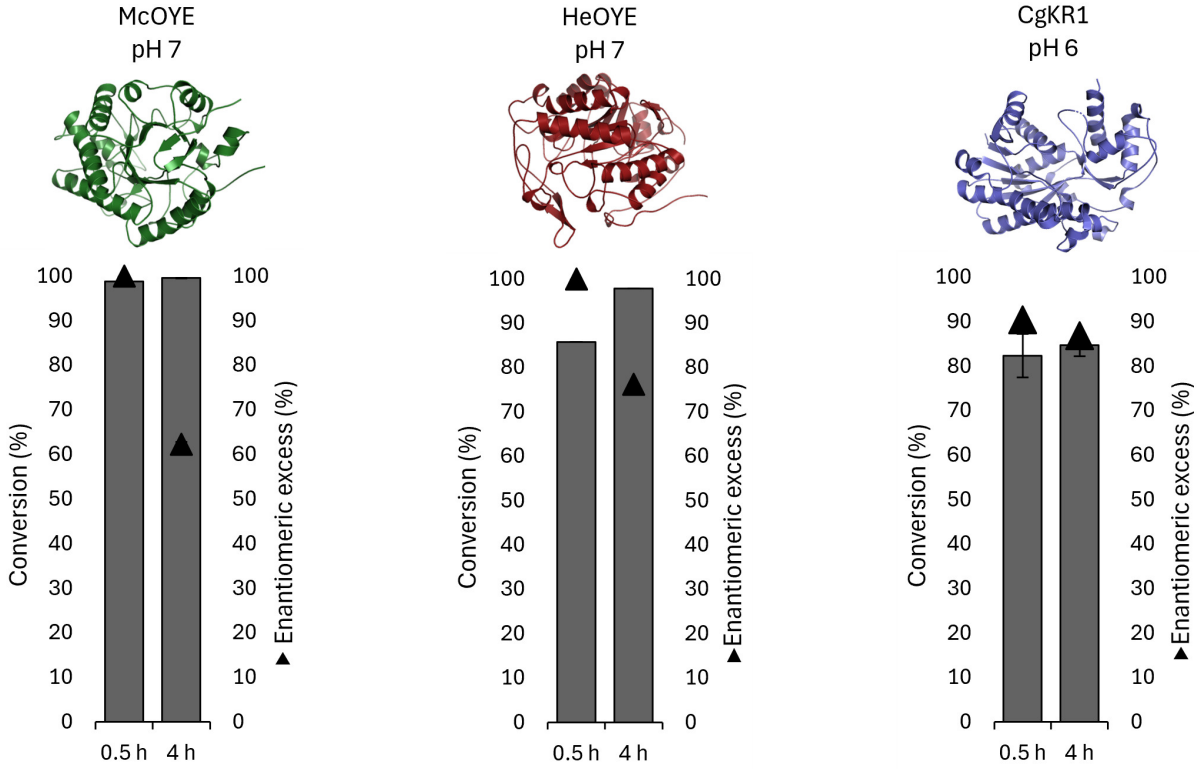

Figure 14: The conversion of the substrate during control reactions with McOYE (left, 4-ketoisophorone), HeOYE (middle, 4-ketoisophorone), and CgKR1 (right, acetophenone), at 0.5 and 4 h. All samples were performed in duplicates, except for HeOYE.

In a first step, we optimized the conditions for the enzymatic control reactions using stoichiometric amounts of NAD(P)H. We chose to employ the enzymes consistently at 0.2 mg/mL. The ratio between enzyme and ^{IR}Resin is a critical parameter in chemo-enzymatic reactions. Thus, we decided to define the amount of enzyme in terms of concentration (mg/mL) rather than enzymatic activity (U). This approach facilitates the comparison between different experiments. Moreover, the similar molecular weights of the three enzymes further simplify direct

comparison between the different systems. We chose to employ the enzymes consistently at 0.2 mg/mL.

We employed an excess of NAD(P)H in all blanks, to ensure that the reaction is not hindered by a lack of NAD(P)H. Both McOYE and CgKR1 reached their maximum conversion after 0.5 h, as there are no differences between a reaction time of 0.5 h and 4 h. This short reaction time resulted in a high enantiomeric excess (e.e.) for both. HeOYE however did not reach full conversion after 0.5 h, making McOYE the better candidate for further optimizations. CgKR1 catalysed the enantioselective reduction of the substrate acetophenone, giving us two different enzyme types to combine with the ^{Ir}Silicycle, ene-reductases and a ketoreductase.

2.11 TM and ^{Ir}Silicycle inhibition of the enzymes

We hypothesized that the immobilized catalyst will have a less inhibitory effect on the enzymatic activity than free TM catalysts like IrPYE-Cl. To test this, we ran enzymatic inhibition control reactions with an excess amount of NAD(P)H, in the presence of free TM catalysts and ^{Ir}Silicycle (Figure 15).

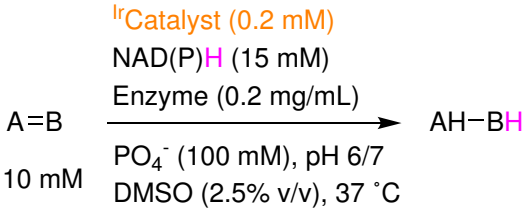

Scheme 18: The scheme of the enzymatic inhibition control reactions, an enantioselective reduction of a substrate *via* an NAD(P)H dependant enzyme. An ^{Ir}Catalyst (IrPYE-Cl or ^{Ir}Silicycle) is added to determine its inhibitory effect on the enzyme.

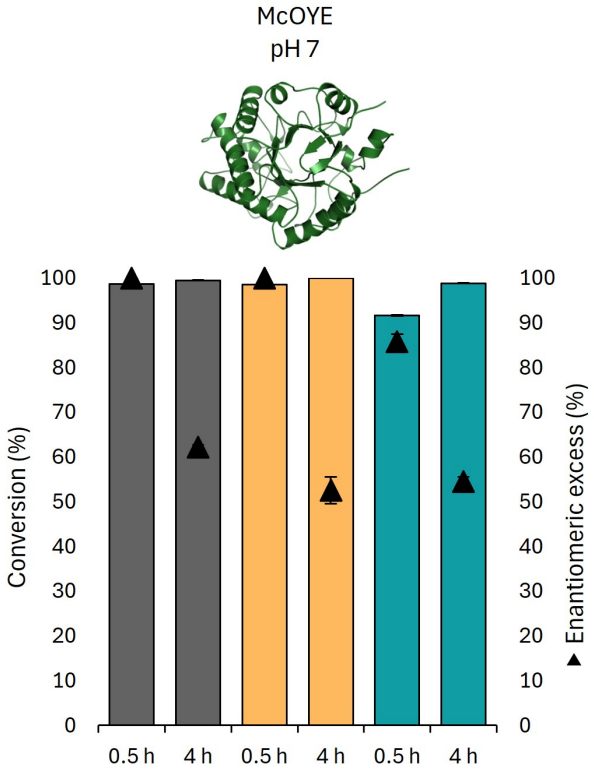

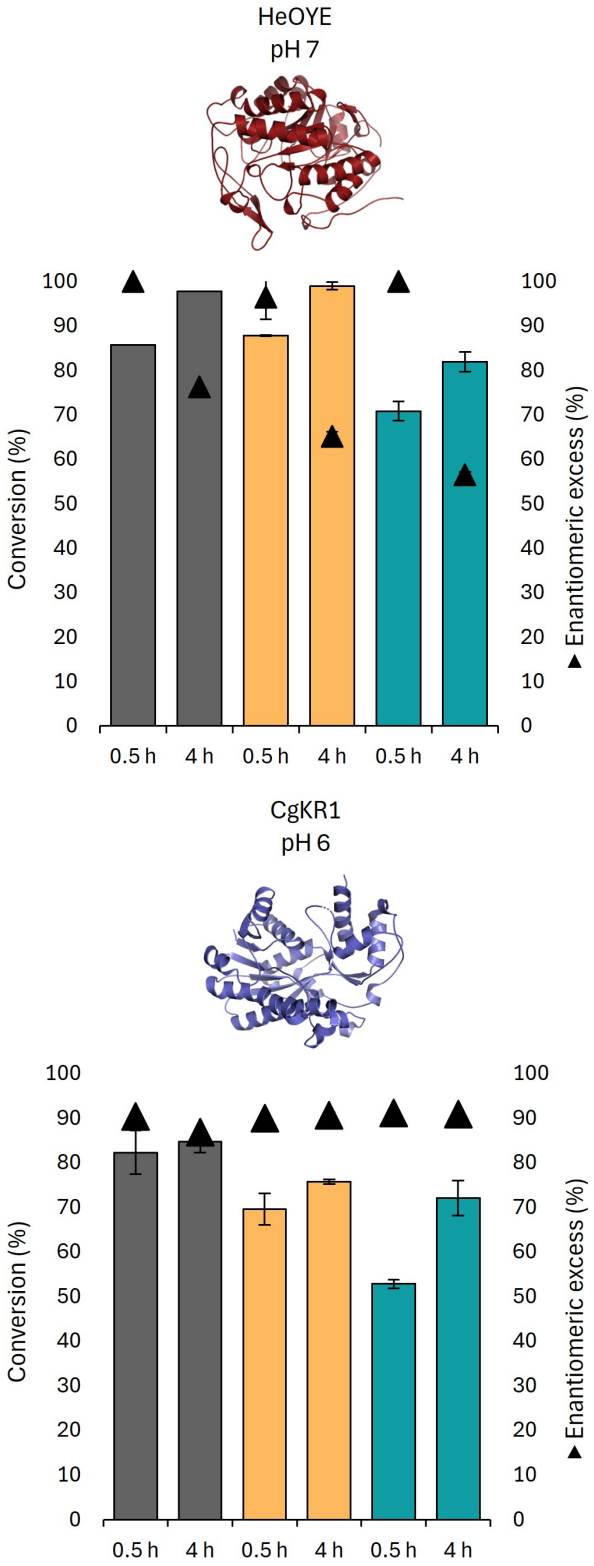

Figure 15: The conversion of the substrate during control reactions (grey), with added ^{Ir}Silicycle (orange), or IrPYE-Cl (turquoise), with different enzymes at 0.5 and 4 h.

We saw no change in the conversion with either McOYE or HeOYE when adding ^{Ir}Silicycle. At both 0.5 h and 4 h, the conversion is identical to the enzymatic control. A slight difference was visible in the e.e. of both after 4 h. This difference in e.e. will be discussed later. CgKR1 showed

a slightly lower conversion after 0.5 h compared to the enzymatic control, some inhibition seems to still be present, despite the reduction in interactions created by the immobilization of the catalyst. It is possible that the surface of CgKR1 possesses more nucleophilic amino acids, potentially coordinating to the immobilized complex, reducing the enzyme's activity.

Free IrPYE-Cl on the other hand clearly inhibited all enzymes. The inhibition with McOYE could clearly be seen, as we reached only 90% conversion after 0.5 h, a 10% difference to the enzymatic controls. The enzyme has seemingly not ceased its catalytic activity, as we still reached full conversion at the 4 h time point.

HeOYE was inhibited even more strongly, as we reached only 71% conversion after 0.5 h, a 15% difference to the enzymatic control. We also no longer reached full conversion after 4 h, but only 82%, an 18% difference. HeOYE seemed to cease its catalytic function sometime after 0.5 h.

CgKR1 was the most inhibited of the three enzymes, reaching only 53% conversion after 0.5 h, a drastic 32% difference to the enzymatic control shown previously. Even after 4 h, we reached only 72% conversion, a 3% difference to the control reaction with the ^{Ir}Silicycle, and still a 12% difference to the enzymatic control.

In conclusion, we circumvented the inhibition of both McOYE and HeOYE by the TM catalyst *via* catalyst immobilization. McOYE was the least inhibited of the three enzymes, showing the lowest inhibition when paired directly with free IrPYE-Cl. These results suggested that McOYE will likely be a viable candidate for chemo-enzymatic reactions.

2.12 Enzymatic inhibition of ^{Ir}Silicycle

As we found conditions that allow for an efficient NADH regeneration and catalyst recycling, we aimed to find out if the ^{Ir}Silicycle is inhibited by the free enzymes. We tested enzyme/complex ratios (1/500), shown in unpublished work by Laura Monte, to lead to minimal mutual inhibition between free enzymes and free TM catalysts (Figure 16).

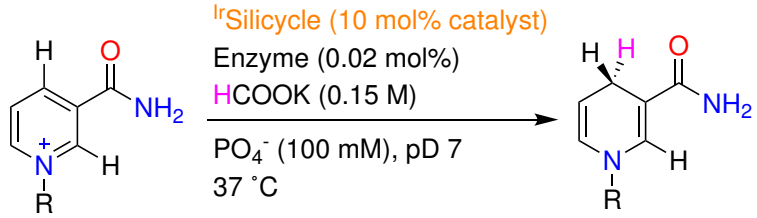

Scheme 19: The scheme of the catalytic regeneration of NADH *via* ^{Ir}Silicycle. A ratio of 1/500 enzyme/complex is established to determine the inhibition of the immobilized catalyst *via* different enzymes.

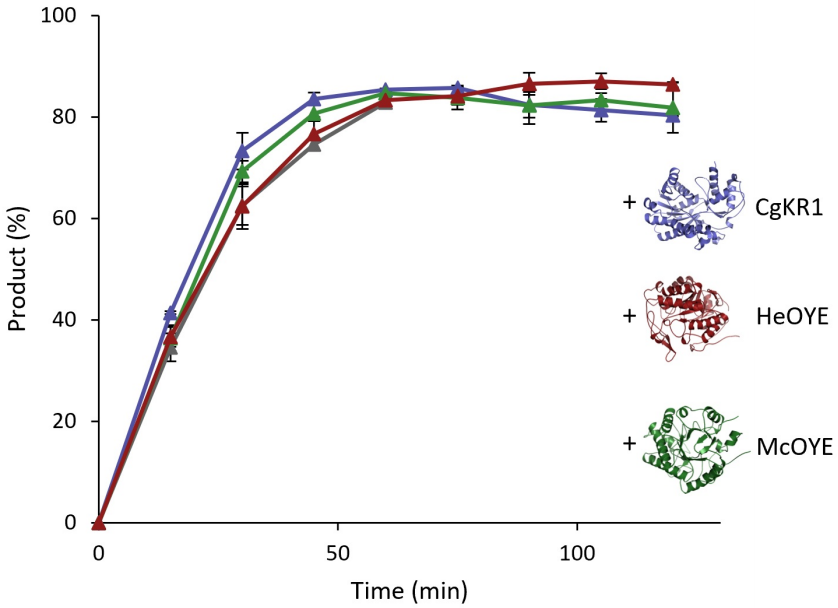

Figure 16: The product of the catalytic regeneration of NADH *via* ^{Ir}Silicycle over time. To determine the inhibition of the ^{Ir}Silicycle (grey) *via* added McOYE (green), HeOYE (red), or CgKR1 (blue), a ratio of 1/500 enzyme/complex is used.

We could not detect any relevant changes at the 1/500 enzyme/complex ratios.

We next tried an enzyme/complex ratio of roughly 1/40 (Figure 17). This ratio would never work in previously reported data, but as we reduced the interactions, we might be able to circumvent it.

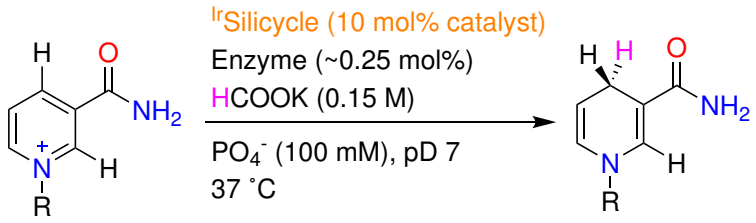

Scheme 20: The scheme of the catalytic regeneration of NADH *via* [Ir]Silicycle. A ratio of roughly 1/40 enzyme/complex is established to determine the inhibition of the immobilized catalyst *via* different enzymes at ratios and conditions for chemo-enzymatic reactions.

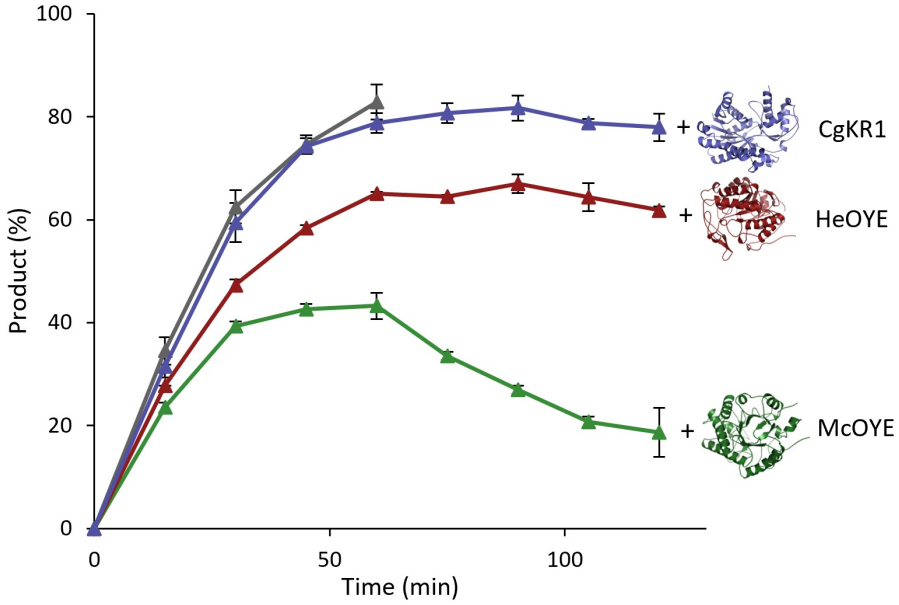

Figure 17: The product of the catalytic regeneration of NADH *via* [Ir]Silicycle over time. To determine the inhibition of the [Ir]Silicycle (grey) *via* added McOYE (green), HeOYE (red), or CgKR1 (blue), a ratio of roughly 1/40 enzyme/complex is used.

As all enzymes have similar molecular weights, the ratios of enzyme/complex stay roughly the same, allowing for proper comparisons.

CgKR1 showed very little to no inhibitory effect, as the amount and speed at which NADH was formed was within error margins to the [Ir]Silicycle sample.

For both McOYE and HeOYE however we could see clear differences in the amount of NADH formed over time. At the 15 min mark, the sample with added McOYE contained a total 10% less NADH than the [Ir]Silicycle sample. After 60 min the sample with added McOYE reached its maximum conversion of 43%. The amount of NADH then started to decline, while the signal for NAD^+ started to increase again. This is unexpected for two reasons: First, we did not add any substrate for McOYE into the sample solution, meaning it does not catalyse a reaction, which could lead to the NADH being used. Second, and more interestingly, McOYE is not NADH dependant, but NADPH! In our previous work we saw only low conversion of the substrate when NADH instead of NADPH was used, demonstrating the specificity of McOYE towards its preferred cofactor. When we compared the results to the previous results of the 1/500 ratio, we hypothesized that the large amount of enzyme present did play a role in the

decrease of NADH, as nothing beyond the ratio has changed. However, we could not conclude, what the exact mechanism behind the observed NADH oxidation is.

HeOYE showed only mild inhibition of the ^{Ir}Silicycle.

The inhibition of the ^{Ir}Silicycle *via* the enzymes stands in direct opposite to the inhibition of the enzymes *via* the ^{Ir}Silicycle. We showed that the enzymatic activity of CgKR1 was the most inhibited by the ^{Ir}Silicycle, but the ^{Ir}Silicycle was the least inhibited by the presence of CgKR1. On the other hand, the exact opposite can be seen when testing McOYE, whose enzymatic activity was not inhibited by the ^{Ir}Silicycle, but the ^{Ir}Silicycle seemed strongly inhibited by the presence of McOYE. Despite these findings, McOYE was still a promising candidate, as all produced NAD(P)H will likely immediately be used. This means we will mostly work at the maximum TOF, which showed only marginal change, no matter the enzyme added. We also showed that the ^{Ir}Silicycle still catalyses the NADH regeneration if relatively large amounts of enzyme are present.

2.13 Chemo-enzymatic reactions with CgKR1

With all the data gathered from previous experiments, we now combined both ^{Ir}Silicycle and enzymes, in chemo-enzymatic reactions. We carried out chemo-enzymatic reactions with CgKR1. CgKR1 showed the lowest inhibition on the ^{Ir}Silicycle, and can be employed for acetophenone reduction.

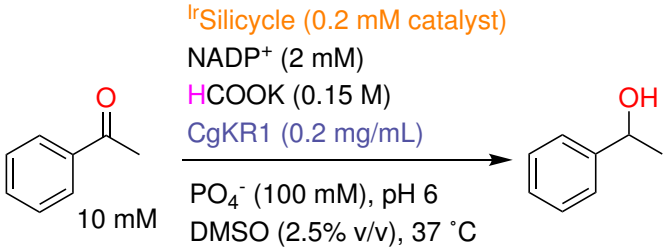

Scheme 21: The schemes of a chemo-enzymatic reaction (10 mol% immobilized catalyst loading) with CgKR1.

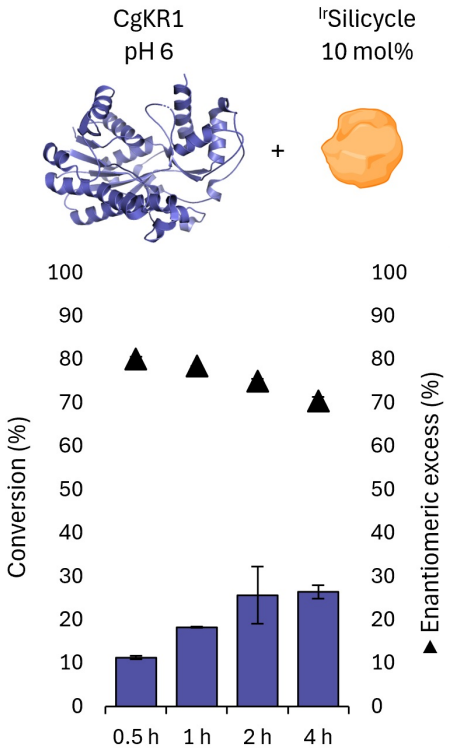

Figure 18: The conversion of a chemo-enzymatic reaction (10 mol% immobilized catalyst loading) with CgKR1, over time.

CgKR1 ceased its catalytic activity after 2 h, as there was no difference in conversion between 2 h and 4 h. To determine if the product had been produced by the enzyme, we ran a background control reaction with the ^{Ir}Silicycle, leaving out solely the enzyme (Figure 19).

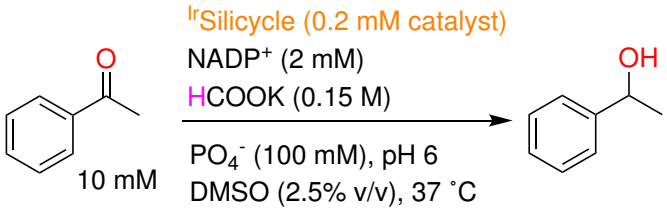

Scheme 22: The scheme of the ^{Ir}Silicycle background control reaction (10 mol% immobilized catalyst loading) of acetophenone.

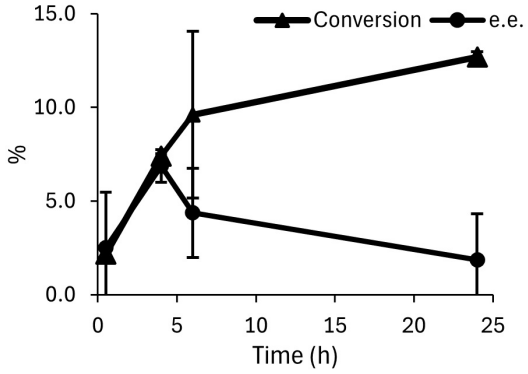

Figure 19: The conversions of a ^{Ir}Silicycle background control reaction (10 mol% immobilized catalyst loading) of acetophenone, over time.

The product was mostly racemic within the error. The reaction duration of the CgKR was only 2 h, as afterwards the enzyme seemingly ceased its catalytic function. This could have been due to two reasons. Either, the enzyme degraded over time, or no more NAD(P)$^+$ was available. While the conversion of acetophenone was considerably higher after 24 h (12.7%), we could still assume less than 5% conversion during the first 4 h. Even with this assumption, this resulted in 80% of the acetophenone being converted by the CgKR1. To determine why conversion stopped after 2 h, the chemo-enzymatic reaction was repeated for a total duration of 4 h. After 2 h, either additional NAD(P)$^+$, additional CgKR1, or both NAD(P)$^+$ and CgKR1, was added (Figure 20).

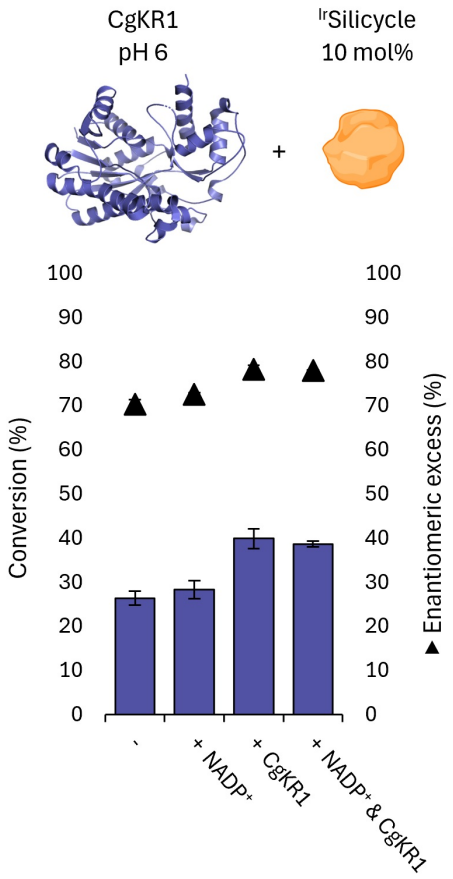

Figure 20: The conversions of chemo-enzymatic reactions (10 mol% immobilized catalyst loading) with CgKR1 (right), over 4 h.

The results suggested that the CgKR1 degraded after 2 h, as the addition of enzyme lead to higher conversion. The addition of solely $NAD(P)^+$ led to no significant changes in conversion. These limitations make CgKR1 unsuitable for these types of chemo-enzymatic reactions, as they would necessitate the constant addition of additional CgKR1. We therefore opted to only continue with McOYE for future chemo-enzymatic reactions.

2.14 Chemo-enzymatic reactions with McOYE

Due to the prior discussed limitations of CgKR1 in chemo-enzymatic reactions, we next employed McOYE, aiming to identify the optimal conditions to achieve high yields and e.e.'s. McOYE showed the lowest inhibition by ^{Ir}Silicycle or IrPYE-Cl. We optimized the ^{Ir}Catalyst loading and the NAD(P)$^+$ concentration.

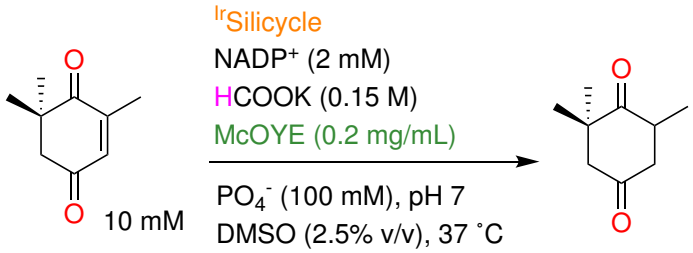

Scheme 23: The scheme of a chemo-enzymatic reaction with McOYE.

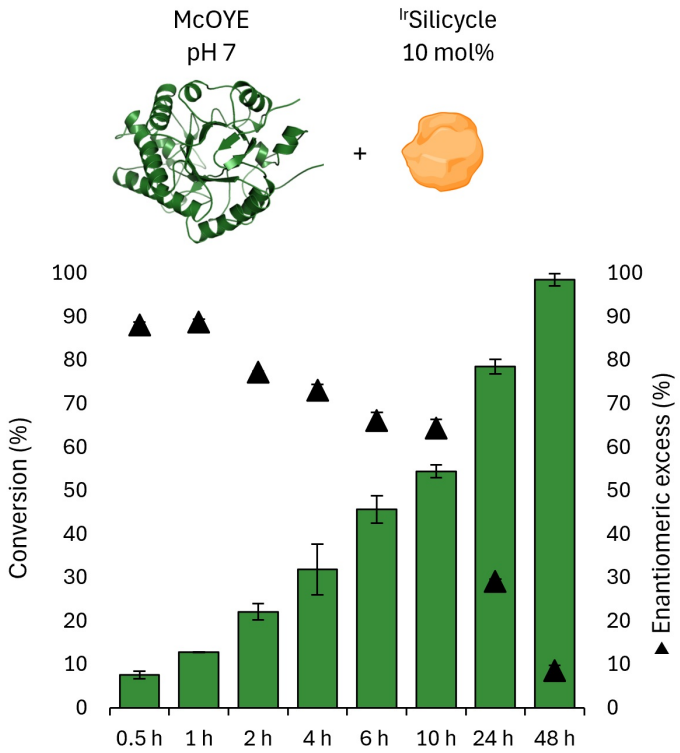

Figure 21: The conversion of a chemo-enzymatic reaction (10 mol% immobilized catalyst loading) with McOYE, over time.

Figure 21 shows full conversion of the substrate after 48 h. Similarly to CgKR1, we wanted to determine if the products had been solely produced by McOYE, and therefore we ran an additional background control reaction with the ^{Ir}Silicycle, leaving out solely McOYE (Figure 22).

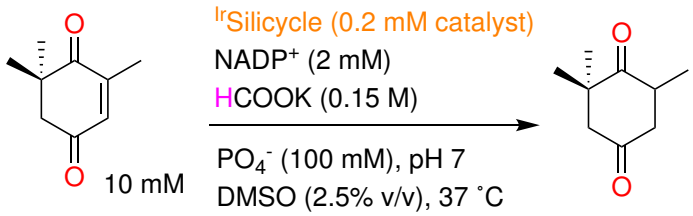

Scheme 24: The scheme of the IrSilicycle background control reaction (10 mol% immobilized catalyst loading) of 4-ketoisophorone.

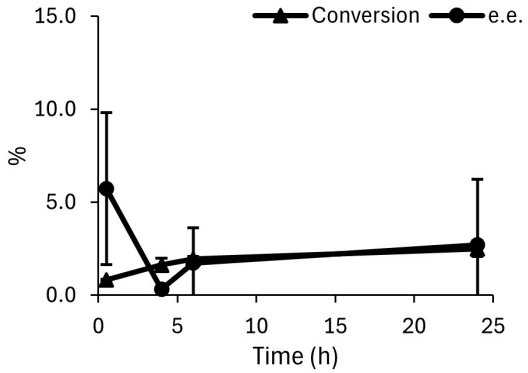

Figure 22: The conversions of a IrSilicycle background control reaction (10 mol% immobilized catalyst loading) of 4-ketoisophorone, over time.

The product produced in these background reactions was mostly racemic within the error, similarly to CgKR1. We measured the conversion of 4-ketoisophorone to be at 2.5% after 24 h. We could safely assume that the conversion during the first 24 h of the chemo-enzymatic reaction was catalysed mainly be the enzyme. Additionally, we hypothesized that the activity of the IrSilicycle does not change after 24 h. Therefore, we assumed that at least 95% of the 4-ketoisophorone was converted by the McOYE.

We hypothesized to reach a higher e.e. by speeding up the NAD(P)$^+$ regeneration. In order to achieve this, we increased the immobilized catalyst loading to 50 mol% (Figure 23).

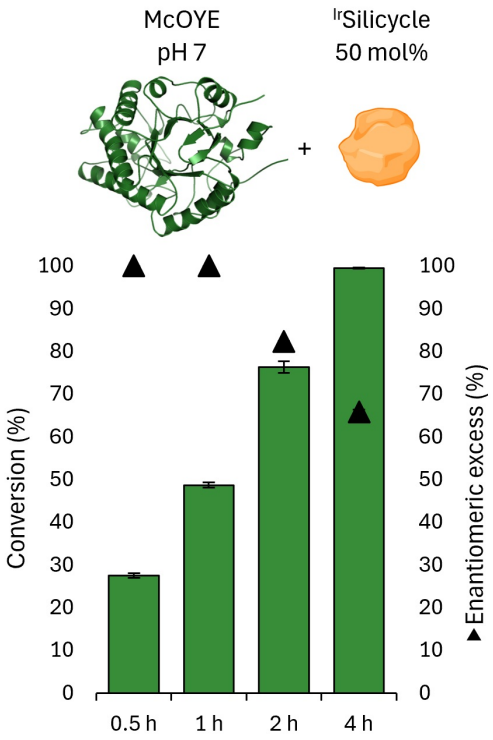

Figure 23: The conversion of a chemo-enzymatic reaction (50 mol% immobilized catalyst loading) with McOYE, over time.

While we cut down the time until reaching full conversion by 90%, down to 4 h, the product started racemizing, still leading to an unsatisfactory e.e. We therefore increased the immobilized catalyst loading to 100 mol% (Figure 24).

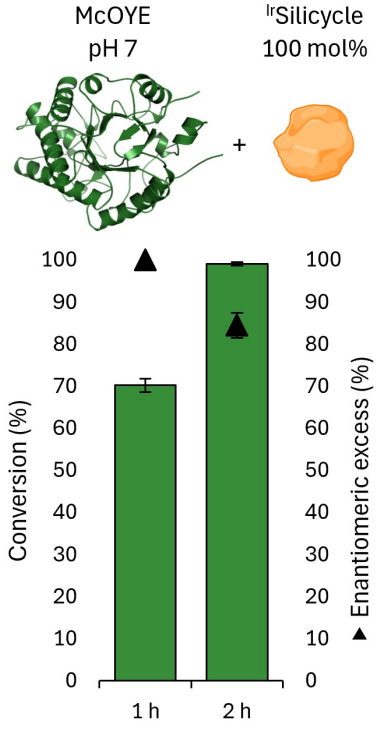

Figure 24: The conversion of a chemo-enzymatic reaction (100 mol% immobilized catalyst loading) with McOYE, over time.

As we reached full conversion after 2 h with an e.e. of 85%, we decided to cycle with these conditions.

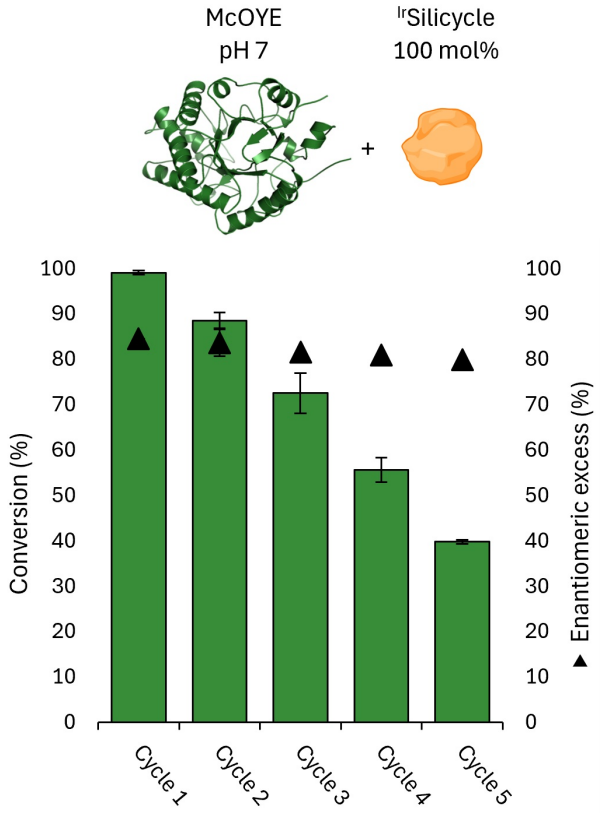

Figure 25: The conversion of a cycled chemo-enzymatic reaction (100 mol% immobilized catalyst loading) with McOYE, for a reaction time of 2 h, over 5 cycles.

Figure 25 shows that the total conversion diminished over the 5 cycles. This was likely due to catalyst leaching, leading to lower catalyst loadings.

We wanted to additionally test if it is possible to lower the amount of $NAD(P)^+$ provided. We only halved the $NAD(P)^+$ amount, leading to a 200 mol% catalyst loading. This reaction however yielded only 76% conversion after 2 h. It is hypothesized that the side reactions have almost completely depleted the available $NAD(P)^+$, as 2 h led to full conversion with double the amount of $NAD(P)^+$ and 100 mol% catalyst loadings.

In order to determine the remaining catalyst on the ^{Ir}Silicycle after the 5 cycles, we lyophilized the used resin, and subsequently determined the amount of immobilized catalyst per gram of dry ^{Ir}Silicycle *via* ICP-MS.

^{Ir}Silicycle Sample	Initial immobilized complex (mg/g dry resin)	Immobilized complex after 5 cycles (mg/g dry resin)
1	48.84±1.06	47.44±19.09
2	48.84±1.06	24.69±2.79

Table 8: The Initial and measured amounts of immobilized complex on the two ^{Ir}Silicycle resins employed during cycled chemo-enzymatic reactions. Samples consist of triplicate measurements.

Sample 1 showed a large standard deviation, which is why it is disregarded during this discussion. Sample 2 however showed expected results, as well as a small standard deviation, further supporting it. With roughly 50% remaining immobilized complex, it is not surprising we recorded a lower conversion, especially in cycle 5. The less immobilized catalyst is present, the slower the NAD(P)H regeneration becomes, leading to a lower conversion over 2 h. If this leaching could be minimized, the speed of the regeneration could be kept consistent for longer. This could be possible with minimizing the amount of time the ^{Ir}Silicycle spends in solution. We therefore hypothesized that reactions in flow with a large excess of ^{Ir}Silicycle could lead to a rapid NAD(P)H regeneration, reducing the time the resin spends in solvent. This could reduce the leaching and prolong the longevity of the resin.

In conclusion, we have found suitable conditions for chemo-enzymatic reactions with McOYE. The reaction could be cycled, and the resin could be reused up to 5 times with acceptable yields and high e.e.'s. Flow chemistry has been hypothesized to be a suitable candidate to potentially prolong the life-span of the resin by reducing the leaching of immobilized catalyst.

2.15 Racemization of 2,2,6-Trimethyl-1,4-cyclohexanedione

With 2,2,6-Trimethyl-1,4-cyclohexanedione we saw racemization over time. The product can undergo racemization in aqueous solutions due to keto-enol tautomerization (Scheme 25). We did however not know if this racemization was catalysed by either the immobilized TM catalyst or McOYE.

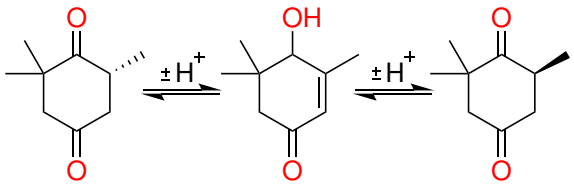

Scheme 25: The keto-enol tautomerism of 2,2,6-Trimethyl-1,4-cyclohexanedione in aqueous solutions.

To determine the influence of both on the speed of racemization, we produced the near enantiopure product with enzymatic control reactions and subsequently extracted and purified it. The product was then added to one of two solutions and kept at 37 °C over time: Solution one consisted of only phosphate buffer. Solution two consisted of phosphate buffer, $NADP^+$, potassium formate, DMSO, ^{Ir}Silicycle, and McOYE, all in the same amounts as they would be present in normal chemo-enzymatic assays. This solution will be called a chemo-enzymatic mimic.

Time (h)	buffer (e.e. %)	chemo-enzymatic mimic (e.e. %)
1	82.2±0.6	86.6±3.1
6	39.5±0.4	40.8±0.8

Table 9: The e.e. of the product of McOYE control reactions over time, after being stored in either only phosphate buffer or a solution mimicking conditions during a chemo-enzymatic reaction.

Table 9 showed no significant difference in e.e. between the conditions, indicating no influence in the speed of racemization by neither the enzyme nor the complex. It is possible that the phosphate buffer has a catalytic influence, but as the buffer was kept constant in all reactions, this influence can be neglected. We conclude that the racemization of the product is not catalysed by neither the immobilized TM complex, nor the enzyme!

2.16 Applications of ^{Ir}Silicycle in flow

^{Ir}Sililcycle already showed good reusability in previous chemo-enzymatic recycling experiments. Moreover, we hypothesized that lower reaction times would improve the longevity of the resin. We therefore employed and optimized the functionalized resin in a flow chemistry setup.

Herein, we optimized the flow setup by testing different flow-rates and co-packing with different resins. The latter is relevant because co-packing allows us to keep a large column volume while using smaller amount of functionalized resin. Moreover, compatibility with different resins is relevant since it enhances potential compatibility with immobilized enzymes.

Co-packing resin	Flow-rate (mL/min)	Residence time (min)	Conversion (%)
Silicycle-OH	0.5	3.4	61±1.1
Silicycle-OH	0.2	8.5	99±0.71
EP400	0.5	3.4	37±1.0
EP400	0.2	8.5	85±1.8

Table 10: Optimization of parameters for the NADH regeneration in flow.

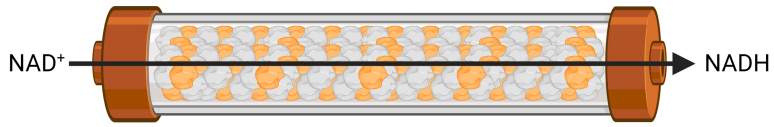

Scheme 26: The scheme of the NADH regeneration in flow. The flow reactor is co-packed with ^{Ir}Silicycle (orange) and either Silicycle-OH or EP400 resin. Created in https://BioRender.com

We first co-packed the ^{Ir}Silicycle with Silicycle-OH resin. The uncharged alcohol modifications are unlikely to interact with NAD^+ nor NADH. It also allowed the creation of a homogeneous slurry with the ^{Ir}Silicycle.

We saw high conversion of NAD^+ into NADH, therefore we decided to increase the total amount of NAD^+

At the same flow-rate, the conversion dropped considerably. We hypothesized to increase conversion by lowering the flow-rate, which will lead to an increased residence time of the solution in the reactor.

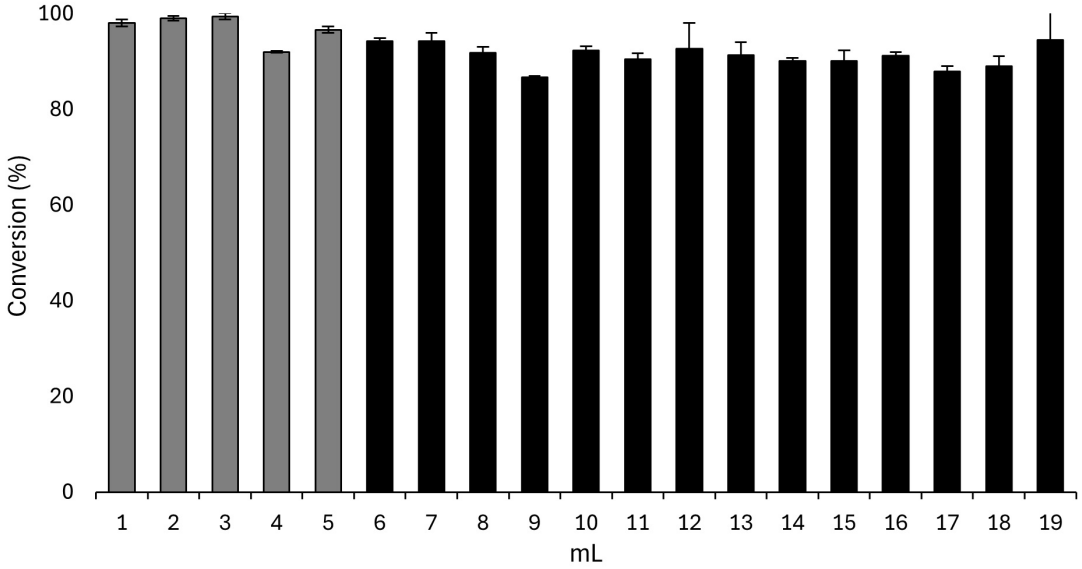

Figure 26: The conversion of a 10 mM NAD^+ solution during NADH regeneration in flow. The reactor was co-packed with Si-Do resin, at a flow-rate of 0.2 mL/min, resulting in a residence time of 8.5 min. After 5 mL (grey), the column was flushed with 10 mL of isopropanol, before the reaction was continued, to determine the column's tolerance towards organic solvents.

With the higher residence time, we reached consistent and high conversions over 19 mL, for a TON of 28 (Figure 26). After the first 5 mL (grey), the column was flushed with isopropanol, to determine if the column tolerates the presence of organic solvents. As there were no relevant differences after these first 5 mL, we argue that the ^{Ir}Silicycle can be further employed even after being flushed with organic solvents.

As the McOYE was immobilized on an EP400 resin, we employed the same resin for co-packing. The resin was however first functionalized to contain alcohol groups *via* treatment with sulfuric acid. The slurry of the ^{Ir}Silicycle and EP400 could not be homogenized, leading to an uneven packing of the column, with visible differences in ^{Ir}Silicycle density. Despite this, we attempted the NADH regeneration.

Even after we lowered the flow rate to increase the residence time, we saw lower overall conversion of NAD^+ than with the Silicycle-OH co-packing. This could have been due to the uneven packing of the column. Alternatively, the different material of the EP400 may have interfered with the substrate to some extent, preventing efficient conversion.

We will co-pack only with Silicycle-OH, as it allowed more reliable co-packing and yields better conversion.

We next employed the immobilized McOYE and checked if it catalyses the desired reduction of 4-ketoisophorone.

Sample	Flow-rate (mL/min)	Residence time (min)	Conversion (%)
1	0.2	8.5	<1
2	0.05	34.2	<1
3	0.02	85.5	<1

Table 11: Optimization of parameters for the enzymatic reduction of 4-ketoisophorone in flow.

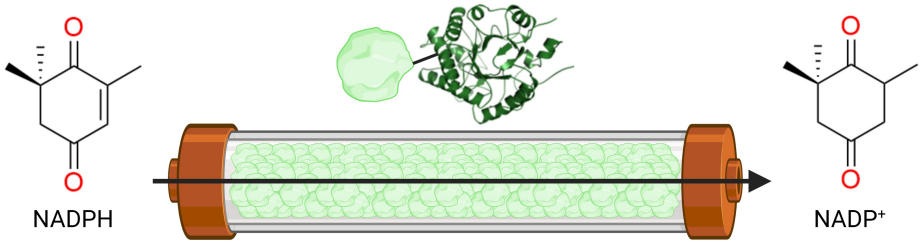

Scheme 27: The scheme of the reduction of 4-ketoisophorone with immobilized McOYE (green). The flow reactor contains solely EP400 resin with immobilized McOYE. Created in https://BioRender.com

However, this immobilized enzyme did not catalyse the reaction, as we could not detect any amounts of product except for background. We lowered the flow-rate to 0.05 mL/min, resulting in a residence time of 34.2 min, but still no product could be detected *via* GC. Further lowering the flow-rate to 0.02 mL/min, the lowest flow-rate possible with the peristaltic pump employed, resulting in a residence time of 85.5 min, again no product could be detected *via* GC.

Due to time constraints, no other enzymes could be immobilized and checked for their proper function in flow. Future experiments could employ enzymes that are known to efficiently catalyse their reaction in flow. They could then be combined with the ^{Ir}Silicycle, co-packed with Si-Do. The NAD(P)H regeneration with the ^{Ir}Silicycle should be very modular, and could therefore be employed with whatever conditions the enzyme requires.

3 Conclusions and outlook

We successfully synthesized two IrPYE variants, both containing electrophilic leaving groups for the purpose of covalent immobilization of the complex. We then immobilized one such IrPYE variant, the IrPYE-Cl, on 4 different resins. To quantify the amount of immobilized complex on the solid support, we successfully developed an aqua regia workflow, which should be applicable to many different immobilized TM catalysts.

All ^{Ir}Resins were then employed in the benchmark aldehyde reduction first. After gauging the activity of the different ^{Ir}Resins, we subsequently tested their activity towards NADH regeneration. The ^{Ir}Silicycle became our resin of choice, due to the relatively high amounts of immobilized complex, its structural stability, and its activity in the NADH regeneration.

We successfully found conditions under which the enzymes we aimed to employ reached full conversion in short time-frames. The ^{Ir}Silicycle, as well as the enzymes, were then tested under the same conditions for mutual inhibition. CgKR1 was least inhibiting the ^{Ir}Silicycle, while the McOYE was least inhibited by the ^{Ir}Silicycle. We could therefore successfully circumvent the issue of mutual inhibition of enzymes and TM catalysis by covalent immobilization of the IrPYE-Cl.

We then combined the ^{Ir}Silicycle and CgKR1 or McOYE. The combination of ^{Ir}Silicycle and McOYE had shown itself to be the most promising, as it reached full conversion after 48 h, with a 10 mol% immobilized catalyst loading. We further established a cycling system, reaching full conversion after 2 h with high e.e., which we employed over 5 cycles. While conversion steadily dropped, likely due to the leaching of immobilized catalyst, we hypothesized to prolong the longevity of the resin by minimizing the time it spends in solvents.

Hence we employed the ^{Ir}Silicycle in flow, where we successfully established a protocol for the regeneration of NADH. This system is likely highly modular and could be combined with many different immobilized NAD(P)H dependent enzymes. We also employed immobilized McOYE, however, we could not detect any conversion in control reactions, so the two immobilized catalysts could not be successfully combined.

In future work, the difference in activity between the immobilized IrPYE-Cl and the immobilized longer chain IrPYE variant (compound **8**) could be explored. As the ligand is modular, a nucleophilic variant could likely be achieved by changing the synthetic procedures, leading to more variety in the accessible solid supports. We also hypothesize that other immobilized NAD(P)H dependent enzymes could easily be combined with the ^{Ir}Silicycle, due to its proposed modularity in flow conditions.

Use of generative AI in scientific writing

In general, the department of Chemistry, Biochemistry and Pharmaceutical sciences allows the use of AI assisted technologies in the preparation of written documents. However, where authors use AI and AI-assisted technologies (e.g. ChatGPT, Google Bard, Microsoft Bing, DeepL, Grammarly, etc.) in the writing process, these technologies should only be used to improve readability and language of the work and not to replace key authoring tasks such as producing scientific insights or drawing scientific conclusions. Applying the technology should be done with human oversight and control and all work should be reviewed and edited carefully. The authors are ultimately responsible and accountable for the contents of the work. Authors should disclose in their written work the use of AI and AI-assisted technologies in a clear statement at the end of text. We recommend placing it before the reference section. If more than one tool was used, they should be listed separately.

Disclosure of use of aimed-assisted technologies

During the preparation of this work, I used the following tools:

1. Google Gemini - LaTeX code generation, as well as improving the readability and language of certain sentences.

After using these tools/services, I reviewed and edited the content as needed and take full responsibility for the content of the publication. I am aware that in case of discompliance, the generated text is considered plagiarism with its legal consequences.

Bibliography

1. Guo, Z., Gao, S., Liu, P., Liu, Y. & Jiang, Y. pH-Responsive aqueous homogeneous metal/enzyme catalysis and heterogeneous recovery enabled by organic cages. *Green Chemistry* **27,** 11429–11437 (2025).
2. Wang, K. *et al.* Overcoming the Limitations of Transition-Metal Catalysis in the Chemoenzymatic Dynamic Kinetic Resolution (DKR) of Atropisomeric Bisnaphthols. *ACS Central Science* **10,** 2099–2110 (2024).
3. Fu, W. *et al.* A metalloenzyme platform for catalytic asymmetric radical dearomatization. *Nature Chemistry,* 1–10 (2024).
4. Wang, C. *et al.* Formate-Mediated Electroenzymatic Synthesis via Biological Cofactor NADH. *Angewandte Chemie International Edition* **63,** e202408756 (2024).
5. Stroek, W., Rowlinson, N. A., Hudson, L. A. & Albrecht, M. Enantioselective C–H amination catalyzed by homoleptic iron salox complexes. *Chemical Communications* **61,** 15274–15277 (2025).
6. Albarrán-Velo, J., González-Martínez, D. & Gotor-Fernández, V. Stereoselective biocatalysis: A mature technology for the asymmetric synthesis of pharmaceutical building blocks. *Biocatalysis and Biotransformation* **36,** 102–130 (2018).
7. Ni, Y., Holtmann, D. & Hollmann, F. How Green is Biocatalysis? To Calculate is To Know. *ChemCatChem* **6** (2014).
8. Anastas, P. & Eghbali, N. Green chemistry: principles and practice. *Chemical society reviews* **39,** 301–312 (2010).
9. Lee, S. H., Kwon, Y.-C., Kim, D.-M. & Park, C. B. Cytochrome P450-catalyzed O-dealkylation coupled with photochemical NADPH regeneration. *Biotechnology and Bioengineering* **110,** 383–390 (2013).
10. Lutz, J. *et al.* Bioorganometallic chemistry: biocatalytic oxidation reactions with biomimetic NAD+/NADH co-factors and [Cp* Rh (bpy) H]+ for selective organic synthesis. *Journal of organometallic chemistry* **689,** 4783–4790 (2004).
11. Hildebrand, F. & Lütz, S. Stable electroenzymatic processes by catalyst separation. *Chemistry–A European Journal* **15,** 4998–5001 (2009).
12. Rodriguez-Alvarez, M. J. *et al.* Combination of metal-catalyzed cycloisomerizations and biocatalysis in aqueous media: Asymmetric construction of chiral alcohols, lactones, and γ-hydroxy-carbonyl compounds. *ACS Catalysis* **7,** 7753–7759 (2017).

13. Sato, H., Hummel, W. & Gröger, H. Cooperative catalysis of noncompatible catalysts through compartmentalization: wacker oxidation and enzymatic reduction in a one-pot process in aqueous media. *Angewandte Chemie International Edition* **54,** 4488–4492 (2015).

14. Poizat, M., Arends, I. W. & Hollmann, F. On the nature of mutual inactivation between [Cp* Rh (bpy)(H2O)] 2+ and enzymes–analysis and potential remedies. *Journal of Molecular Catalysis B: Enzymatic* **63,** 149–156 (2010).

15. Keller, R. F. *Exploring the uses of an IrPYE+/IrPYEH complex in NAD(P)+/NAD(P)H dependent ene-reductase reactions* Bachelor's Thesis (2024).

16. Cortes-Clerget, M. *et al.* Bridging the gap between transition metal-and bio-catalysis via aqueous micellar catalysis. *Nature communications* **10,** 2169 (2019).

17. Paris, J. *et al.* Enantioselective one-pot synthesis of biaryl-substituted amines by combining palladium and enzyme catalysis in deep eutectic solvents. *ACS Sustainable Chemistry & Engineering* **7,** 5486–5493 (2019).

18. Cicco, L. *et al.* Programming cascade reactions interfacing biocatalysis with transition-metal catalysis in Deep Eutectic Solvents as biorenewable reaction media. *Green Chemistry* **20,** 3468–3475 (2018).

19. Ríos-Lombardía, N. *et al.* DES ign of Sustainable One-Pot Chemoenzymatic Organic Transformations in Deep Eutectic Solvents for the Synthesis of 1, 2-Disubstituted Aromatic Olefins. *Frontiers in Chemistry* **8,** 139 (2020).

20. Whitehurst, D. D. & Haag, W. O. *German pat.* 1,8000,371 (1969).

21. Barker, H., Garnett, J., Levot, R. & Long, M. Use of Additives to Enhance Radiation Grafting of Monomers to Polyvinyl Chloride) and Application of These PVC Copolymers to Immobilization of Enzymes and Heterogenization of Homogeneous Metal Complexes. *Journal of Macromolecular Science—Chemistry* **12,** 261–273 (1978).

22. Garber, S. B., Kingsbury, J. S., Gray, B. L. & Hoveyda, A. H. Efficient and recyclable monomeric and dendritic Ru-based metathesis catalysts. *Journal of the American Chemical Society* **122,** 8168–8179 (2000).

23. Mayr, M., Buchmeiser, M. R. & Wurst, K. Synthesis of a Silica-Based Heterogeneous Second Generation Grubbs Catalyst. *Advanced Synthesis & Catalysis* **344,** 712–719 (2002).

24. Halbach, T. S. *et al.* Novel ruthenium-based metathesis catalysts containing electron-withdrawing ligands: synthesis, immobilization, and reactivity. *The Journal of Organic Chemistry* **70,** 4687–4694 (2005).

25. Vehlow, K., Maechling, S., Köhler, K. & Blechert, S. Versatile Ru-based metathesis catalysts designed for both homogeneous and heterogeneous processes. *Journal of organometallic chemistry* **691,** 5267–5277 (2006).

26. Pugin, B. & Blaser, H.-U. The Immobilization of Rhodium-4-(diphenylphosphino)-2-(diphenylphosphinomethyl)-pyrrolidine (Rh-PPM) Complexes: A Systematic Study. *Advanced Synthesis & Catalysis* **348,** 1743–1751 (2006).

27. Allen, D. P., Van Wingerden, M. M. & Grubbs, R. H. Well-defined silica-supported olefin metathesis catalysts. *Organic letters* **11,** 1261–1264 (2009).

28. Joya, K. S., Subbaiyan, N. K., D'Souza, F. & de Groot, H. J. Surface-immobilized single-site iridium complexes for electrocatalytic water splitting. *Angewandte Chemie-International Edition* **51,** 9601 (2012).

29. Samantaray, M. K. *et al.* Evidence for metal–surface interactions and their role in stabilizing well-defined immobilized Ru–NHC alkene metathesis catalysts. *Journal of the American Chemical Society* **135,** 3193–3199 (2013).

30. Liu, X., Maegawa, Y., Goto, Y., Hara, K. & Inagaki, S. Heterogeneous catalysis for water oxidation by an iridium complex immobilized on bipyridine-periodic mesoporous organosilica. *Angewandte Chemie International Edition* **55,** 7943–7947 (2016).

31. Hübner, S., de Vries, J. G. & Farina, V. Why does industry not use immobilized transition metal complexes as catalysts? *Advanced Synthesis & Catalysis* **358,** 3–25 (2016).

32. Nguyen, H. H. & Kim, M. An overview of techniques in enzyme immobilization. *Applied Science and Convergence Technology* **26,** 157–163 (2017).

33. Homaei, A. Enzyme immobilization and its application in the food industry. *Advances in food biotechnology,* 145–164 (2015).

34. Gianfreda, L. & Scarfi, M. R. Enzyme stabilization: state of the art. *Molecular and cellular biochemistry* **100,** 97–128 (1991).

35. Mateo, C., Palomo, J. M., Fernandez-Lorente, G., Guisan, J. M. & Fernandez-Lafuente, R. Improvement of enzyme activity, stability and selectivity via immobilization techniques. *Enzyme and microbial technology* **40,** 1451–1463 (2007).

36. Wu, J. C. Y., Hutchings, C. H., Lindsay, M. J., Werner, C. J. & Bundy, B. C. Enhanced enzyme stability through site-directed covalent immobilization. *Journal of biotechnology* **193,** 83–90 (2015).

37. Cunha, A. G. *et al. Immobilization of Yarrowia lipolytica lipase—a comparison of stability of physical adsorption and covalent attachment techniques* in *Biotechnology for Fuels and Chemicals: Proceedings of the Twenty-Ninth Symposium on Biotechnology for Fuels and Chemicals Held April 29–May 2, 2007, in Denver, Colorado* (2007), 169–176.

38. Zhang, D.-H., Yuwen, L.-X. & Peng, L.-J. Parameters affecting the performance of immobilized enzyme. *Journal of chemistry* **2013,** 946248 (2013).

39. Gelati, L., Gervasini, A., Paradisi, F., Speranza, G., *et al.* in *XLIX "A. CORBELLA" INTERNATIONAL SUMMER SCHOOL ON ORGANIC SYNTHESIS* (2025).

40. Truppo, M. D. & Hughes, G. Development of an improved immobilized CAL-B for the enzymatic resolution of a key intermediate to odanacatib. *Organic Process Research & Development* **15,** 1033–1035 (2011).

41. Padrosa, D. R., Benítez-Mateos, A. I., Calvey, L. & Paradisi, F. Cell-free biocatalytic syntheses of l-pipecolic acid: A dual strategy approach and process intensification in flow. *Green chemistry* **22,** 5310–5316 (2020).

42. Contente, M. L. & Paradisi, F. Self-sustaining closed-loop multienzyme-mediated conversion of amines into alcohols in continuous reactions. *Nature Catalysis* **1,** 452–459 (2018).

43. Haraldsson, G. G., Halldorsson, A. & Thorstad, O. *US Patent* 7,491,522 B2 (2009).

44. Mohamad, N. R., Marzuki, N. H. C., Buang, N. A., Huyop, F. & Wahab, R. A. An overview of technologies for immobilization of enzymes and surface analysis techniques for immobilized enzymes. *Biotechnology & Biotechnological Equipment* **29,** 205–220 (2015).

45. Imam, H. T., Marr, P. C. & Marr, A. C. Enzyme entrapment, biocatalyst immobilization without covalent attachment. *Green Chemistry* **23,** 4980–5005 (2021).

46. Wu, J. T., Wu, L. H. & Knight, J. A. Stability of NADPH: effect of various factors on the kinetics of degradation. *Clinical chemistry* **32,** 314–319 (1986).

47. Weckbecker, A. & Hummel, W. in *Microbial enzymes and biotransformations* 225–238 (Springer, 2005).

48. Liu, F. *et al.* Electrocatalytic NAD+ reduction via hydrogen atom-coupled electron transfer. *Chemical Science* **13,** 13361–13367 (2022).

49. Morrison, C. S., Armiger, W. B., Dodds, D. R., Dordick, J. S. & Koffas, M. A. Improved strategies for electrochemical 1, 4-NAD (P) H2 regeneration: A new era of bioreactors for industrial biocatalysis. *Biotechnology Advances* **36,** 120–131 (2018).

50. Immanuel, S., Sivasubramanian, R., Gul, R. & Dar, M. A. Recent progress and perspectives on electrochemical regeneration of reduced nicotinamide adenine dinucleotide (NADH). *Chemistry–An Asian Journal* **15,** 4256–4270 (2020).

51. Ruppert, R., Herrmann, S. & Steckhan, E. Efficient indirect electrochemical in-situ regeneration of nadh: electrochemically driven enzymatic reduction of pyruvate catalyzed by d-ldh. *Tetrahedron Letters* **28,** 6583–6586 (1987).

52. Tensi, L. & Macchioni, A. Extremely fast NADH-regeneration using phosphonic acid as hydride source and iridium-pyridine-2-sulfonamidate catalysts. *ACS Catalysis* **10,** 7945–7949 (2020).

53. Trotta, C., Menendez Rodriguez, G., Zuccaccia, C. & Macchioni, A. Electrochemical NADH regeneration mediated by pyridine amidate iridium complexes interconverting 1, 4-and 1, 6-NADH. *ACS Catalysis* **14,** 10334–10343 (2024).

54. Trotta, C. *et al.* Organometallic Catalysis Catches up with Enzymatic in the Regeneration of NADH. *ACS catalysis* **15,** 9417–9429 (2025).

55. Rodriguez, G. M., Trotta, C., Tensi, L. & Macchioni, A. Reversible Electrocatalytic NAD+/NADH Interconversion Mediated by a Pyrazine-Amidate Iridium Complex. *Journal of the American Chemical Society* **146,** 34298–34303 (2024).

56. Lentz, N. & Albrecht, M. A low-coordinate iridium complex with a donor-flexible O, N-ligand for highly efficient formic acid dehydrogenation. *ACS Catalysis* **12,** 12627–12631 (2022).

57. Lentz, N., Reuge, S. & Albrecht, M. NADH-Type Hydride Storage and Release on a Functional Ligand for Efficient and Selective Hydrogenation Catalysis. *ACS Catalysis* **13,** 9839–9844 (2023).

58. Wang, D. & Astruc, D. The golden age of transfer hydrogenation. *Chemical reviews* **115,** 6621–6686 (2015).

59. Benítez-Mateos, A. I. & Paradisi, F. Sustainable flow-synthesis of (bulky) nucleoside drugs by a novel and highly stable nucleoside phosphorylase immobilized on reusable supports. *ChemSusChem* **15,** e202102030 (2022).

60. Cayot, P. & Tainturier, G. The quantification of protein amino groups by the trinitrobenzenesulfonic acid method: a reexamination. *Analytical biochemistry* **249,** 184–200 (1997).

61. Burnett, J. W. *et al.* Directing the H 2-driven selective regeneration of NADH via Sn-doped Pt/SiO 2. *Green Chemistry* **24,** 1451–1455 (2022).

Erklärung

gemäss Art. 30 RSL Phil.-nat.18

Name/Vorname: Keller Robin Frédéric

Matrikelnummer: 21-103-726

Studiengang: Molecular Life Sciences: Biochemistry/Chemical Biology

Bachelor ☐ Master ☑ Dissertation ☐

Titel der Arbeit: Synthesis and Immobilization of an Iridium Complex for use in Enzymatic Biocatalysis

LeiterIn der Arbeit: Martin Albrecht

Ich erkläre hiermit, dass ich diese Arbeit selbständig verfasst und keine anderen als die angegebenen Quellen benutzt habe. Alle Stellen, die wörtlich oder sinngemäss aus Quellen entnommen wurden, habe ich als solche gekennzeichnet. Mir ist bekannt, dass andernfalls der Senat gemäss Artikel 36 Absatz 1 Buchstabe r des Gesetzes vom 5. September 1996 über die Universität zum Entzug des auf Grund dieser Arbeit verliehenen Titels berechtigt ist.
Für die Zwecke der Begutachtung und der Überprüfung der Einhaltung der Selbständigkeitserklärung bzw. der Reglemente betreffend Plagiate erteile ich der Universität Bern das Recht, die dazu erforderlichen Personendaten zu bearbeiten und Nutzungshandlungen vorzunehmen, insbesondere die schriftliche Arbeit zu vervielfältigen und dauerhaft in einer Datenbank zu speichern sowie diese zur Überprüfung von Arbeiten Dritter zu verwenden oder hierzu zur Verfügung zu stellen.

Bern, 30.1.26

Ort/Datum

Unterschrift